cmgh
CELLULAR AND MOLECULAR GASTROENTEROLOGY AND HEPATOLOGY

ORIGINAL RESEARCH

Targeting USP9X–AMPK Axis in ARID1A-Deficient Hepatocellular Carcinoma

Feng-Kun Zhang,[1,*] Qian-Zhi Ni,[1,2,*] Kang Wang,[2] Hui-Jun Cao,[1] Dong-Xian Guan,[1] Er-Bin Zhang,[1] Ning Ma,[1] Yi-Kang Wang,[1] Qian-Wen Zheng,[1,3] Sheng Xu,[1] Bing Zhu,[1] Tian-Wei Chen,[1] Ji Xia,[1] Xiao-Song Qiu,[1,3] Xu-Fen Ding,[1] Hao Jiang,[4] Lin Qiu,[1] Xiang Wang,[5] Wei Chen,[6] Shu-Qun Cheng,[2] Dong Xie,[1,3,7,§] and Jing-Jing Li[1,§]

[1]*CAS Key Laboratory of Nutrition, Metabolism and Food Safety, Shanghai Institute of Nutrition and Health, University of Chinese Academy of Sciences, Chinese Academy of Sciences, Shanghai, China;* [2]*Department of Hepatic Surgery VI, Eastern Hepatobiliary Surgery Hospital, Naval Medical University, Shanghai, China;* [3]*School of Life Science and Technology, Shanghai Tech University, Shanghai, China;* [4]*Department of Biomedical Informatics, School of Life Sciences, Central South University, Changsha, Hunan, China;* [5]*Key Laboratory of Integrated Oncology and Intelligent Medicine of Zhejiang Province. Affiliated Hangzhou First People's Hospital, Zhejiang University School of Medicine, Hangzhou, Zhejiang, China;* [6]*Cancer Institute of Integrated Traditional Chinese and Western Medicine, Tongde Hospital of Zhejiang Province, Hangzhou, Zhejiang, China;* [7]*National Health Commission Key Laboratory of Food Safety Risk Assessment, China National Center for Food Safety Risk Assessment, Beijing, China*

SUMMARY

AT-rich interaction domain 1A loss renders hepatocellular carcinoma cells resistant to glucose deprivation via the ubiquitin-specific peptidase 9 X-linked–adenosine 5'-monophosphate–activated protein kinase axis, providing a synthetic lethal therapeutic strategy for AT-rich interaction domain 1A–deficient hepatocellular carcinoma.

BACKGROUND & AIMS: Hepatocellular carcinoma (HCC) is a highly heterogeneous solid tumor with high morbidity and mortality. AT-rich interaction domain 1A (ARID1A) accounts for up to 10% of mutations in liver cancer, however, its role in HCC remains controversial, and no targeted therapy has been established.

METHODS: The expression of ARID1A in clinical samples was examined by Western blot and immunohistochemical staining. ARID1A was knocked out by Clustered Regularly Interspaced Short Palindromic Repeats (CRISPR)/CRISPR-associated protein 9 (Cas9) in HCC cell lines, and the effects of glucose deprivation on cell viability, proliferation, and apoptosis were measured. Mass spectrometry analysis was used to find ARID1A-interacting proteins, and the result was verified by co-immunoprecipitation and Glutathione S Transferase (GST) pull-down. The regulation of ARID1A target gene *USP9X* was investigated by chromatin immunoprecipitation, Glutathione S Transferase (GST) pull-down, luciferase reporter assay, and so forth. Finally, drug treatments were performed to explore the therapeutic potential of the agents targeting ARID1A-deficient HCC in vitro and in vivo.

RESULTS: Our study has shown that ARID1A loss protected cells from glucose deprivation–induced cell death. A mechanism study disclosed that AIRD1A recruited histone deacetylase 1 via its C-terminal region DUF3518 to the promoter of *USP9X*, resulting in down-regulation of USP9X and its target protein kinase AMP-activated catalytic subunit α2 (PRKAA2). ARID1A knockout and a 1989* truncation mutant in HCC abolished this effect, increased the levels of H3K9 and H3K27 acetylation at the *USP9X* promoter, and up-regulated the expression of USP9X and protein kinase AMP-activated catalytic subunit α2 (PRKAA2), which mediated the adaptation of tumor cells to glucose starvation. Compound C dramatically inhibited the growth of ARID1A-deficient tumors and prolongs the survival of tumor-bearing mice.

CONCLUSIONS: HCC patients with ARID1A mutation may benefit from synthetic lethal therapy targeting the ubiquitin-specific peptidase 9 X-linked (USP9X)–adenosine 5'-monophosphate–activated protein kinase (AMPK) axis. *(Cell Mol Gastroenterol Hepatol 2022;14:101–127; https://doi.org/10.1016/j.jcmgh.2022.03.009)*

Keywords: SWI/SNF Complex; HDAC1; Epigenetic.

Liver cancer is one of the most common malignancies in the world, and hepatocellular carcinoma (HCC) patients in China account for approximately 50% of all cases

***Authors share co-first authorship; §Authors share co-senior authorship.**

Abbreviations used in this paper: **AMPK, adenosine 5'-monophosphate–activated protein kinase; ARID1A, AT-rich interaction domain 1A; BSA, bovine serum albumin; ChIP, chromatin immunoprecipitation; co-IP, co-immunoprecipitation; CRISPR, clustered regularly interspaced short palindromic repeats; FBS, fetal bovine serum; GST, glutathione s transferase; HCC, hepatocellular carcinoma; HDAC1, histone deacetylase 1; KO, knockout; mRNA, messenger RNA; MTT, 3-(45)-dimethylthiahiazo (-z-y1)-35-di- phenytetrazoliumromide; PBS, phosphate-buffered saline; PCR, polymerase chain reaction; PRKAA1, protein kinase AMP-activated catalytic subunit α1; PRKAA2, protein kinase AMP-activated catalytic subunit α2; SDS, sodium dodecyl sulfate; shRNA, short hairpin RNA; SWI/SNF, switch/sucrose nonfermentable; TMA, tissue microarray; USP9X, ubiquitin-specific peptidase 9 X-linked; WT, wild-type.**

Most current article

2352-345X
https://doi.org/10.1016/j.jcmgh.2022.03.009

worldwide.[1] Most advanced HCC patients with no surgery option often accept targeted therapy,[2,3] including sorafenib, regorafenib, and lenvatinib.[4] Although these drugs induce an optimal response at the initial stage, most patients develop disease progression, and the drugs have very limited survival benefits.[5] Therefore, development of new therapeutic strategies is needed to improve treatment efficacy in HCC.

AT-rich interaction domain 1A (ARID1A) is a member of the switch/sucrose nonfermentable (SWI/SNF) chromatin remodeling complex, which regulates various biological processes, including DNA replication, DNA transcription, and telomere elongation.[6–8] ARID1A has been identified as one of the most frequently mutated genes by next-generation sequencing in a variety of cancers, including ovarian clear-cell carcinoma, gastric cancer, breast cancer, and so forth.[9] In liver cancer patients, a mutation frequency of approximately 10% was observed for ARID1A.[10,11] Therefore, ARID1A is often considered as a tumor-suppressor gene. However, the role of ARID1A in HCC is complicated, and its function remains largely elusive.[9,12–16]

Adenosine 5'-monophosphate–activated protein kinase (AMPK) is a heterologous trimer complex composed of a catalytic subunit (α) and 2 regulatory subunits (β and γ),[17,18] acting as a key regulator of cellular energy metabolism. Tumor cells consume a large amount of glucose during rapid proliferation, and the AMPK signaling pathway is abnormally activated as a result of energy stress, maintaining tumor growth by controlling metabolic activity, autophagy process, and cell death.[19–22]

In this study, we reported the clinical significance of ARID1A in HCC, as well as its role in regulating the adaptation of cancer cells to low-glucose condition, and clarified the underlying mechanism, providing a novel synthetic lethality strategy for ARID1A-deficient HCC patients.

Results

ARID1A Is Significantly Down-Regulated in HCC and Decreased Expression of ARID1A Is Correlated With a Poor Prognosis

The expression of ARID1A was examined in 18 pairs of HCC tissues and the matched adjacent noncancreous tissues by Western blot, and decreased protein levels of ARID1A in HCC tissues were observed in 15 pairs, accounting for 83% of the total samples (Figure 1*A*). Down-regulation of ARID1A was further identified by immunohistochemical staining (Figure 1*B*).

To explore the clinical significance of ARID1A in HCC, a tissue microarray (TMA) consisting of 243 HCC samples and some matched normal tissues were stained with ARID1A antibody, and the signal density was analyzed by Vectra (Perkin-Elmer, Waltham, MA) (Figure 1*C*). ARID1A was down-regulated in HCC tissues compared with their normal counterparts (Figure 1*D*). We further analyzed the correlation between ARID1A expression and the clinical parameters of HCC patients. Low expression of ARID1A was significantly associated with short overall and disease-free survival of HCC patients (Figure 1*E* and *F*). Patients with low ARID1A expression had more ascites, larger tumor volume, and, more importantly, significantly shorter recurrence-free intervals (Table 1).

Mutation may be one reason for the decreased protein level of ARID1A in HCC. Data from the The Cancer Genome Atlas (TCGA)-Firehose Legacy (N = 373) sample database showed that patients with ARID1A mutations had shorter overall and disease-free survival (Figures 1*G* and *H* and 2*A*). However, the mutation status had little effect on transcription (Figure 2*B*). Therefore, our data showed that either low-protein expression or mutation of ARID1A was significantly correlated with a poor prognosis of HCC patients.

ARID1A Deletion Renders Tumor Cells Resistant to Glucose Deprivation via Activation of AMPK Pathway

The clinical data indicated that ARID1A may be a tumor suppressor. To identify this hypothesis, ARID1A was knocked out by CRISPR/Cas9 in 3 HCC cells with high ARID1A level, including Huh7, YY-8103, and MHCC97H cells, and was overexpressed in SNU-398 and PVTT cells with low ARID1A expression (Figure 2*C* and *D*). In accordance with previous reports,[7,16,23] 3-(4,5-Dimethylthiazol-2-yl)-2,5-diphenyltetrazolium bromide (MTT) and crystal violet assay showed that knockout of ARID1A did not enhance cell proliferation and clonogenic capability, and overexpression of ARID1A in PVTT and SNU-398 cells also showed no significant effect (Figure 2*E–J*). Most cancer cells possess a feature called the Warburg effect, showing high reliance on glucose. Glucose supply in many solid tumors is poor, and exhaustion of glucose by cancer cells with high glycolytic capacity often leads to cell death.[24] Therefore, we examined the response of control, ARID1A knockout (KO), and ARID1A-overexpressing cells to glucose deprivation. When glucose in the medium was reduced, ARID1A KO cells showed significantly higher viability than control cells, indicating that ARID1A KO HCC cells had a survival advantage under glucose deprivation (Figure 3*A–E*). On the other hand, glucose starvation accelerated the death of ARID1A-overexpressing PVTT cells (Figure 3*F* and *G*). However, there was no difference in the response to serum deprivation between control, ARID1A KO, and ARID1A-overexpressing cells (Figure 3*H* and *I*). In addition, knockout of ARID1A suppressed apoptosis in glucose-deficient medium (Figure 4*A* and *B*). Thus, ARID1A deficiency rendered HCC cells resistant to glucose deprivation.

It has been reported that low glucose can activate the AMPK signaling pathway,[20,24–26] so we examined whether ARID1A influenced AMPK activation. As expected, Ampk signaling pathway was obviously activated, associated with increased expression of Ampkα in the livers of *Arid1a* liver-specific KO mice (Figure 4*C* and *D*). AMPKα has 2 isoforms, α1 and α2, encoded by *PRKAA1* and *PRKAA2*, respectively. We further identified that the increased level of Ampkα was attributed to the up-regulation of Prkaa2 in mouse livers (Figure 4*C*), and a similar alteration was observed in ARID1A KO HCC

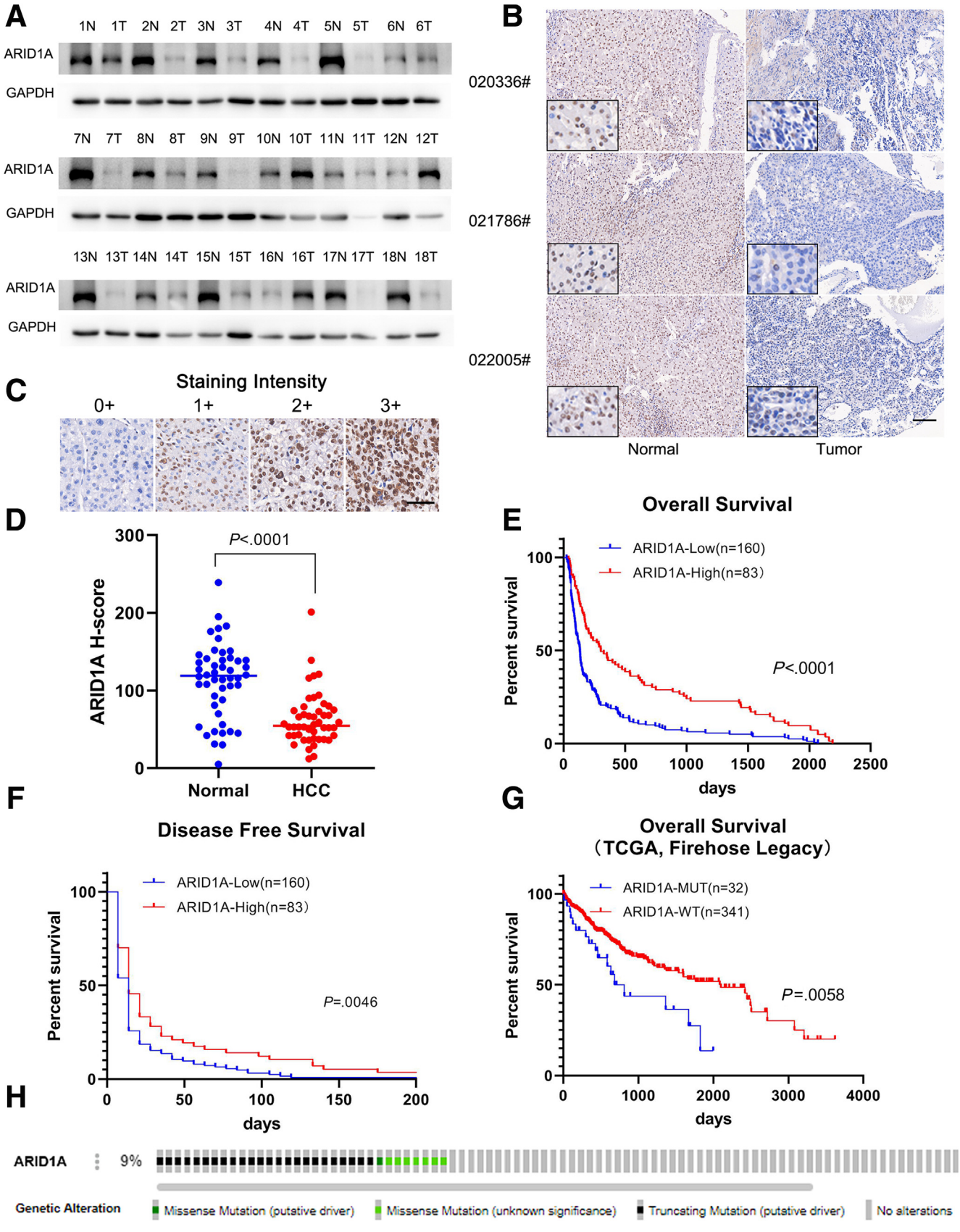
A
1N 1T 2N 2T 3N 3T 4N 4T 5N 5T 6N 6T
ARID1A
GAPDH
7N 7T 8N 8T 9N 9T 10N 10T 11N 11T 12N 12T
ARID1A
GAPDH
13N 13T 14N 14T 15N 15T 16N 16T 17N 17T 18N 18T
ARID1A
GAPDH
B
020336#
021786#
022005#
Normal
Tumor
C
Staining Intensity
0+ 1+ 2+ 3+
D
P<.0001
ARID1A H-score
300
200
100
0
Normal
HCC
E
Overall Survival
ARID1A-Low(n=160)
ARID1A-High(n=83)
Percent survival
100
50
0
P<.0001
0 500 1000 1500 2000 2500
days
F
Disease Free Survival
ARID1A-Low(n=160)
ARID1A-High(n=83)
Percent survival
100
50
0
P=.0046
0 50 100 150 200
days
G
Overall Survival
(TCGA, Firehose Legacy)
ARID1A-MUT(n=32)
ARID1A-WT(n=341)
Percent survival
100
50
0
P=.0058
0 1000 2000 3000 4000
days
H
ARID1A
9%
Genetic Alteration
Missense Mutation (putative driver)
Missense Mutation (unknown significance)
Truncating Mutation (putative driver)
No alterations

Table 1. Relationship Between ARID1A Expression and Clinical Pathologic Features of HCC Patients

Characteristic	Total (N = 243)	Low expression (n = 160)	High expression (n = 83)	χ^2	*P* value
Tumor size (cm)					
≤5	37	18	19	5.738	.017[a]
>5	206	142	64		
TNM stage					
I	33	16	17	5.116	.024[a]
II–IV	210	144	66		
Ascity					
No	187	129	58	3.558	.059
Yes	56	31	25		
Tumor number					
≤1	219	143	76	0.295	.587
>1	24	17	7		
Liver cirrhosis					
No	168	115	53	1.647	.199
Yes	75	45	30		
Relapse					
No	62	36	26	2.24	.135
Yes	181	124	57		
Relapse-free interval (month)					
≤10	165	117	48	4.987	.026[a]
>10	16	7	9		

NOTE. Statistical analyses were performed using the chi-squared test.
[a]$P < .05$ was considered significant.

cells (Figure 4*E*). In contrast, ARID1A overexpression reduced the expression of protein kinase AMP-activated catalytic subunit α 2 (PRKAA2) (Figure 4*F*). *Arid1a* KO did not affect the expression of Ampk upstream kinase Lkb1, as well as Prkaa1 (Figure 4*C*). In addition, the messenger RNA (mRNA) levels of *Prkaa1* and *Prkaa2* were not changed (Figure 4*G* and *H*), indicating that ARID1A may affect AMPKα expression at the post-translational level.

To clarify the role of AMPK in glucose reliance regulated by ARID1A, we constructed 2 short hairpin RNA (shRNA), sh1# and sh2#, respectively, to knocked down PRKAA2 (Figure 5*A*). Down-regulation of PRKAA2 slightly reduced the clonogenic growth of ARID1A KO HCC cells in normal condition, while the growth advantage of ARID1A KO cells in low-glucose condition was abolished by PRKAA2 knockdown (Figure 5*B*). Compound C is the only AMPK inhibitor currently available, which competitively binds adenosine triphosphate and inhibits AMPK kinase activity (Figure 5*C*). Once AMPK was inhibited, the survival advantage of ARID1A KO cells in low-glucose condition was abrogated, which was similar to PRKAA2 knockdown (Figure 5*D* and *F*). Furthermore, ARID1A KO HCC cells were more sensitive to Compound C in normal condition (Figure 5*E* and *G*), with lower half maximal inhibitory concentration (IC_{50}) values when compared with control cells (Figure 5*H–J*). Therefore, the resistance to glucose insufficiency endowed by ARID1A deficiency was dependent on PRKAA2, which rendered the ARID1A-deficient cells more vulnerable to AMPK inhibitor.

ARID1A Regulates the Ubiquitination of PRKAA2 Through Ubiquitin-Specific Peptidase 9 X-Linked (USP9X)

Because Arid1a did not affect the mRNA level of *Prkaa2*, we checked the effect of ARID1A on protein stability of PRKAA2. The ubiquitination of endogenous PRKAA2 was increased dramatically in the presence of ARID1A and MG132, a cell-permeable proteasome inhibitor (Figure 6*A–C*), while PRKAA2 ubiquitination was reduced significantly in ARID1A KO Huh7 cells (Figure 6*D*), indicating that ARID1A could affect ubiquitination of PRKAA2 and regulate its protein stability.

Figure 1. (***See previous page***). **Expression pattern and clinical significance of ARID1A in HCC.** (*A*) Western blot analysis of ARID1A expression in 18 pairs of noncancerous liver tissues (N) and the matched HCC (T) tissues. Glyceraldehyde-3-phosphate dehydrogenase (GAPDH) is used as internal control. (*B*) Immunohistochemistry staining of ARID1A in 3 pairs of HCC tissues and the matched noncancerous liver tissues. *Scale bars*: 100 μm. (*C*) The immunohistochemical scoring criteria for TMA. (*D*) H-scores of ARID1A protein in HCC tissues and the paired noncancerous liver tissues, N = 48. (*E*) Overall survival and (*F*) disease-free survival curve of patients in the ARID1A low (n = 160) and high (n = 83) groups. Data are analyzed using the Student's t test. (*G*) The overall survival curve of HCC patients based on the mutation status of ARID1A, wild-type (n = 341), and mutation (n = 32) from the TCGA–Firehose Legacy data set. (*H*) Mutations of ARID1A in HCC from the TCGA–Firehose Legacy data set. WT, wild-type, MUT, mutation.

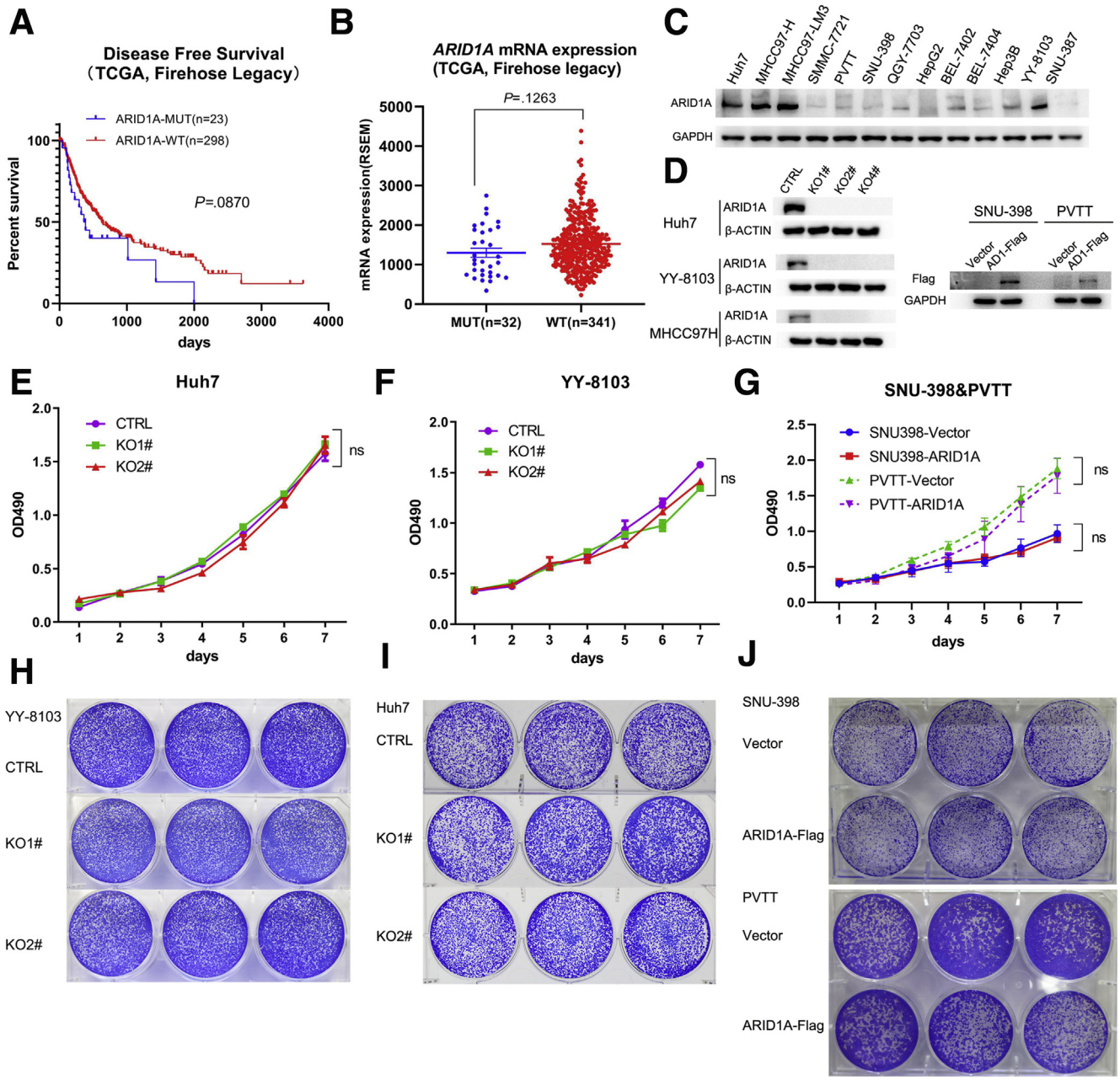

Figure 2. ARID1A deletion does not impair the proliferation of HCC cells. (*A*) The disease-free survival of patients based on the mutation status of ARID1A (TCGA–Firehose Legacy, ARID1A WT, n = 298; ARID1A mutation, n = 23; *P* = .0870). (*B*) ARID1A mutation does not influence the mRNA level in Firehose legacy from the TCGA database. (*C*) The expression of ARID1A in HCC cell lines is examined by Western blot. (*D*) Knockout (*left*) or overexpression (*right*) of ARID1A is examined by Western blot. β-actin or glyceraldehyde-3-phosphate dehydrogenase (GAPDH) is used as internal control. The proliferation of (*E*) ARID1A KO Huh7, (*F*) YY-8103, and (*G*) ARID1A-overexpressing SNU-398, PVTT cells is examined by MTT assay. (*H–J*) The colony-formation ability of (*H*) ARID1A KO YY-8103, (*I*) Huh7, and (*J*) ARID1A-overexpressing SNU-398, PVTT cells is examined by crystal violet assay. CTRL, control; MUT, mutation; RSEM, RNA-Seq expression estimation by expectation-maximization.

Because ARID1A is not a documented ubiquitinase or deubiquitinase, we speculated that the post-translational modification of PRKAA2 was mediated by other molecules. We examined the already known molecules involved in the ubiquitination of AMPKα, including *Usp10*, *Ube2o*, *Cidec*, and *Mkrn1*,[27–30] but found that their mRNA level was not significantly influenced by Arid1a in mouse livers (Figure 6*E*). WP1130, an inhibitor of ubiquitin-specific peptidase 9 X-linked (USP9X), was reported to inhibit the AMPK signaling pathway and down-regulate the protein level of AMPKα, but the mechanism is unclear.[31] Interestingly, we found that liver-specific knockout of Arid1a or

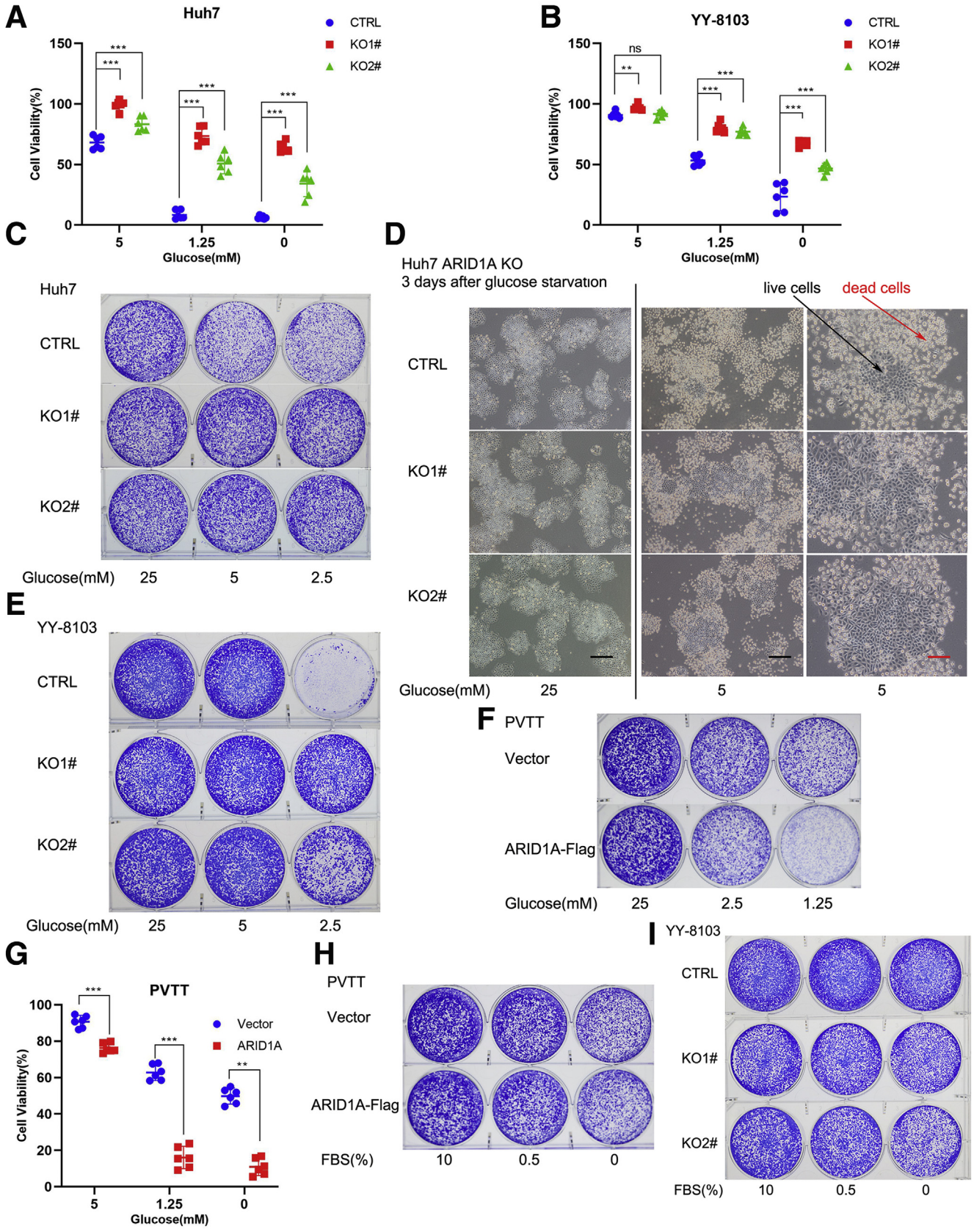
A
Huh7
CTRL
KO1#
KO2#
Cell Viability(%)
Glucose(mM)
B
YY-8103
ns
C
Huh7
CTRL
KO1#
KO2#
Glucose(mM) 25 5 2.5
D
Huh7 ARID1A KO
3 days after glucose starvation
live cells
dead cells
Glucose(mM) 25 5 5
E
YY-8103
F
PVTT
Vector
ARID1A-Flag
Glucose(mM) 25 2.5 1.25
G
PVTT
Vector
ARID1A
H
FBS(%) 10 0.5 0
I
YY-8103

ARID1A knockout in Huh7 and YY-8103 cells significantly increased the mRNA (Figure 6*F*) and protein (Figure 6*G* and *H*) levels of USP9X, while overexpression of ARID1A in SNU-398 cells significantly decreased the protein level of USP9X (Figure 6*I*), which was consistent with the finding of Schick et al.[32] In addition, ARID1A knockout in MHCC97H cells significantly increased the protein level of USP9X and PRKAA2 (Figure 6*J*).

USP9X is a deubiquitination enzyme, and to confirm whether PRKAA2 is a substrate of USP9X, HEK293T cells were transfected with HA-Ub and Vector/USP9X–Flag. As expected, overexpression of USP9X reduced ubiquitination of PRKAA2 (Figure 7*A*). We overexpressed PRKAA2-HA in HEK293T cells, co-immunoprecipitation (co-IP) experiment identified the interaction between USP9X and PRKAA2 (Figure 7*B*), and immunofluorescence experiments showed colocalization of the 2 molecules (Figure 7*C*). Knockdown of USP9X inhibited the expression of PRKAA2 in Huh7 cells (Figure 7*D*). In addition, the USP9X inhibitor WP1130 enhanced PRKAA2 ubiquitination (Figure 7*E*). For further verification, we constructed a loss-of-function USP9X mutant C1566S[33,34] with a C-terminal myc tag, then transfected HEK293T cells with HA-Ub and wild-type (WT)/C1566S USP9X-myc plasmids. In contrast to WT USP9X, C1566S mutant could not attenuate ubiquitination of PRKAA2 (Figure 7*F*). It was reported that the ubiquitination sites of PRKAA2 were K364/K379/K470.[29] We constructed single amino acid mutants of these 3 sites, namely K364R, K379R, and K470R, respectively. WT PRKAA2 and 3 mutants with Flag tag were transfected into HEK293T cells in the presence of WP1130, and only the ubiquitination level of K364R did not change (Figure 7*E*), suggesting that K364 was the specific deubiquitination site in PRKAA2 for USP9X. Based on our finding, we treated control and ARID1A KO Huh7/YY-8103 cells with WP1130 in either normal or low-glucose condition. WP1130 abolished the survival advantage of ARID1A KO HCC cells in low-glucose media (Figure 7*G* and *H*), and it was worthy to note that WP1130 could specifically inhibit cell viability of ARID1A KO cells in normal condition (Figure 7*I* and *J*), suggesting that ARID1A loss sensitizes HCC cells to the inhibition of the USP9X–AMPK axis.

ARID1A Interacts With Histone Deacetylase 1 Through its C-Terminal Domain to Regulate the Expression of USP9X

SWI/SNF complex could recruit histone-modifying enzymes to regulate transcription of target genes.[32] To search for the partner of ARID1A in the regulation of *USP9X*, ARID1A–Flag was overexpressed in HEK293T cells and mass spectrometry analysis of co-immunoprecipitates was performed. The results showed that ARID1A interacted with several SWI/SNF components, such as SWI/SNF related, matrix associated, actin dependent regulator of chromatin, subfamily a, member 4 (SMARCA4/BRG1), SWI/SNF related, matrix associated, actin dependent regulator of chromatin, subfamily a, member 2 (SMARCA2), SWI/SNF related, matrix associated, actin dependent regulator of chromatin subfamily c member 1 (SMARCC1), SWI/SNF related, matrix associated, actin dependent regulator of chromatin, subfamily d, member 2 (SMARCD2), and so forth, which validated the experiment. In addition, we found histone deacetylase 1 (HDAC1) in the list (Figure 8*A*), an important epigenetic regulator often abnormally expressed in tumors. We confirmed the interaction between ARID1A and HDAC1 by co-IP and GST pull-down assay (Figure 8*B*–*E*), and immunofluorescence experiments identified their colocalization in the nucleus (Figure 8*F*). To further clarify their interaction, we constructed 3 mutants of ARID1A with deletion of different domains, including 1-881, 882-1108, and 1109-2285 (Figure 8*G*). The co-IP experiment in HEK293T and PVTT cells showed that when the 1109–2285 region was deleted, the interaction between ARID1A and HDAC1 was abolished, while the other 2 mutants were still able to interact with HDAC1 (Figure 8*H* and *I*). The 1022–2285 region contains the DUF3518 domain, so we cloned the DUF3518 domain separately and verified its interaction with HDAC1 (Figure 8*H* and *I*). Interestingly, we found a mutation (ARID1A-1989*) lacking the DUF3518 domain from the Catalogue of Somatic Mutations in Cancer database, which showed the highest mutation frequency and was also detected in HCC (Figure 9*A*). We constructed this mutant (ARID1A-1989*), and found that it failed to interact with HDAC1 (Figure 9*B*) and was unable to increase the ubiquitination of PRKAA2 like WT ARID1A (Figure 9*C*).

To explore how ARID1A regulates the transcription of *USP9X*, first we cloned the promoter region of human *USP9X* and found that overexpression of ARID1A/HDAC1 in HEK293T and PVTT cells suppressed the promoter activity of *USP9X* (Figure 9*D* and *E*), while Knockout of ARID1A in Huh7 and YY-8103 cells enhanced the promoter activity of *USP9X* (Figure 9*F*). ARID1A-1989* could not influence the promoter activity of *USP9X* (Figure 9*D*), suggesting that ARID1A–HDAC1 interaction was required for the regulation of *USP9X*. Consequently, ARID1A-1989* also failed to decrease the expression of USP9X and PRKAA2 like WT ARID1A (Figure 9*G*).

Figure 3. (***See previous page***). **ARID1A deletion sustains HCC cell survival in low-glucose condition.** Cell viability of control and ARID1A KO (*A*) Huh7 and (*B*) YY-8103 cells under glucose starvation for 48 hours is examined by cell counting kit-8 (CCK8) assay. (*C* and *E*) The crystal violet staining and (*D*) microscopic images of control and ARID1A KO Huh7/YY-8103 cells under glucose starvation. *Black scale bars*: 250 μm; *red scale bars*: 100 μm. (*F*) The crystal violet staining of ARID1A-overexpressing PVTT cells upon glucose starvation. (*G*) The effect of ARID1A overexpression on PVTT cell viability upon glucose starvation is examined by CCK8 assay. The effect of serum deprivation on (*H*) control and ARID1A-overexpressing PVTT or (*I*) ARID1A KO YY-8103 cells, respectively, is examined by crystal violet assay. CTRL, control. $^{**}P<0.01$, $^{***}P<0.001$, ns, not significant.

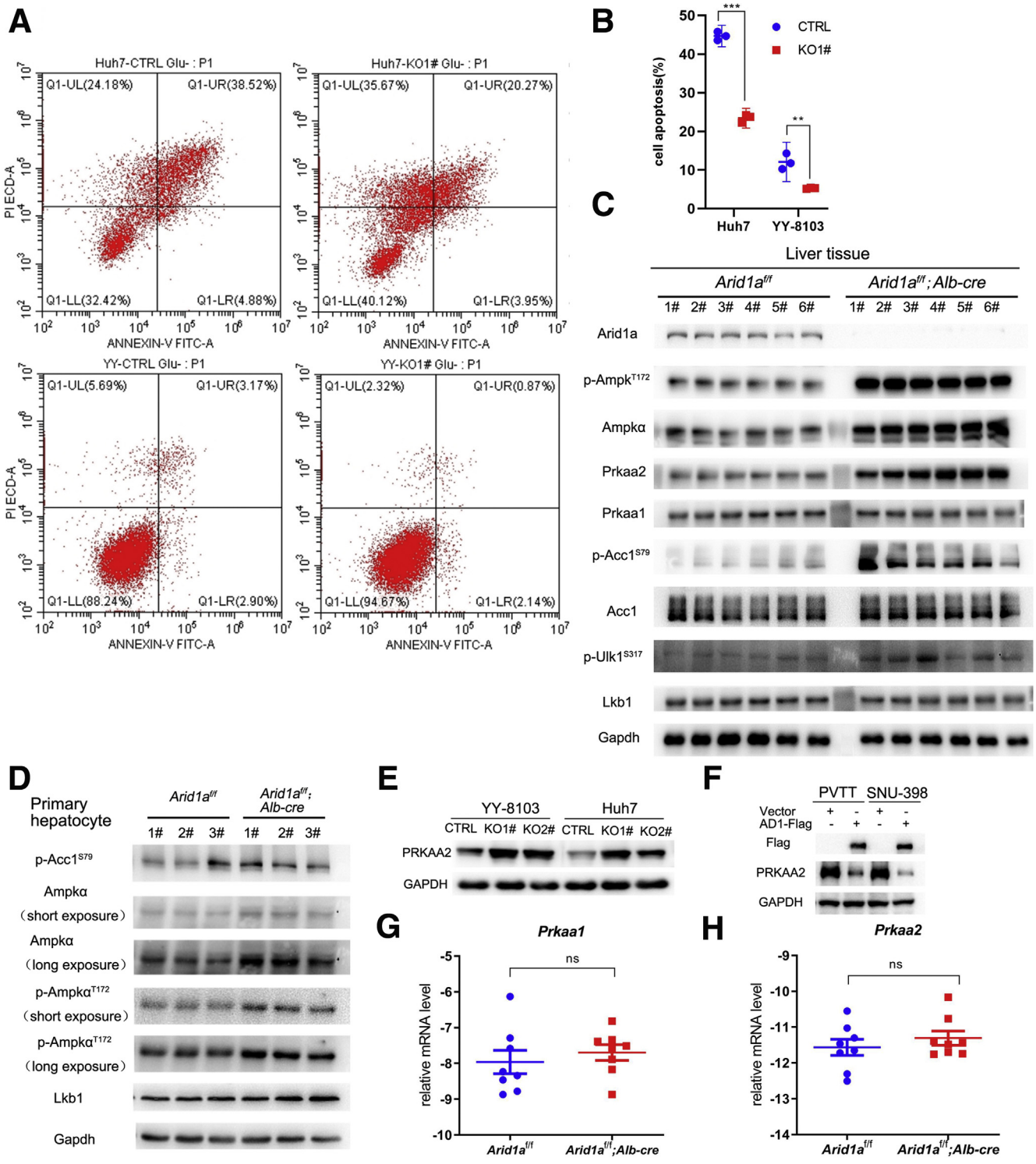

Figure 4. ARID1A deletion renders HCC cells resistant to glucose deprivation via activation of the AMPK pathway. The effect of ARID1A knockout on Huh7 and YY-8103 cells upon glucose starvation is investigated by (*A*) Annexin V–fluorescein isothiocyanate (FITC)/PI apoptosis kit, and (*B*) the result of quantitative analysis is shown. (*C*) The expression of AMPK signaling proteins in liver tissues from control and *Arid1a* liver-specific knockout mice. (*D*) The expression of the indicated proteins in AMPK signaling in primary hepatocytes from control and *Arid1a* liver-specific KO mice. The expression of (*E*) PRKAA2 in control, ARID1A knockout YY-8103, Huh7 cells and (*F*) ARID1A-overexpressing PVTT and SNU-398 cells. The mRNA level of (*G*) *Prkaa1* and (*H*) *Prkaa2* in liver tissues from control and *Arid1a* liver-specific knockout mice. CTRL, control; GAPDH, glyceraldehyde-3-phosphate dehydrogenase. **P*<0.05, ****P*<0.001, ns, not significant.

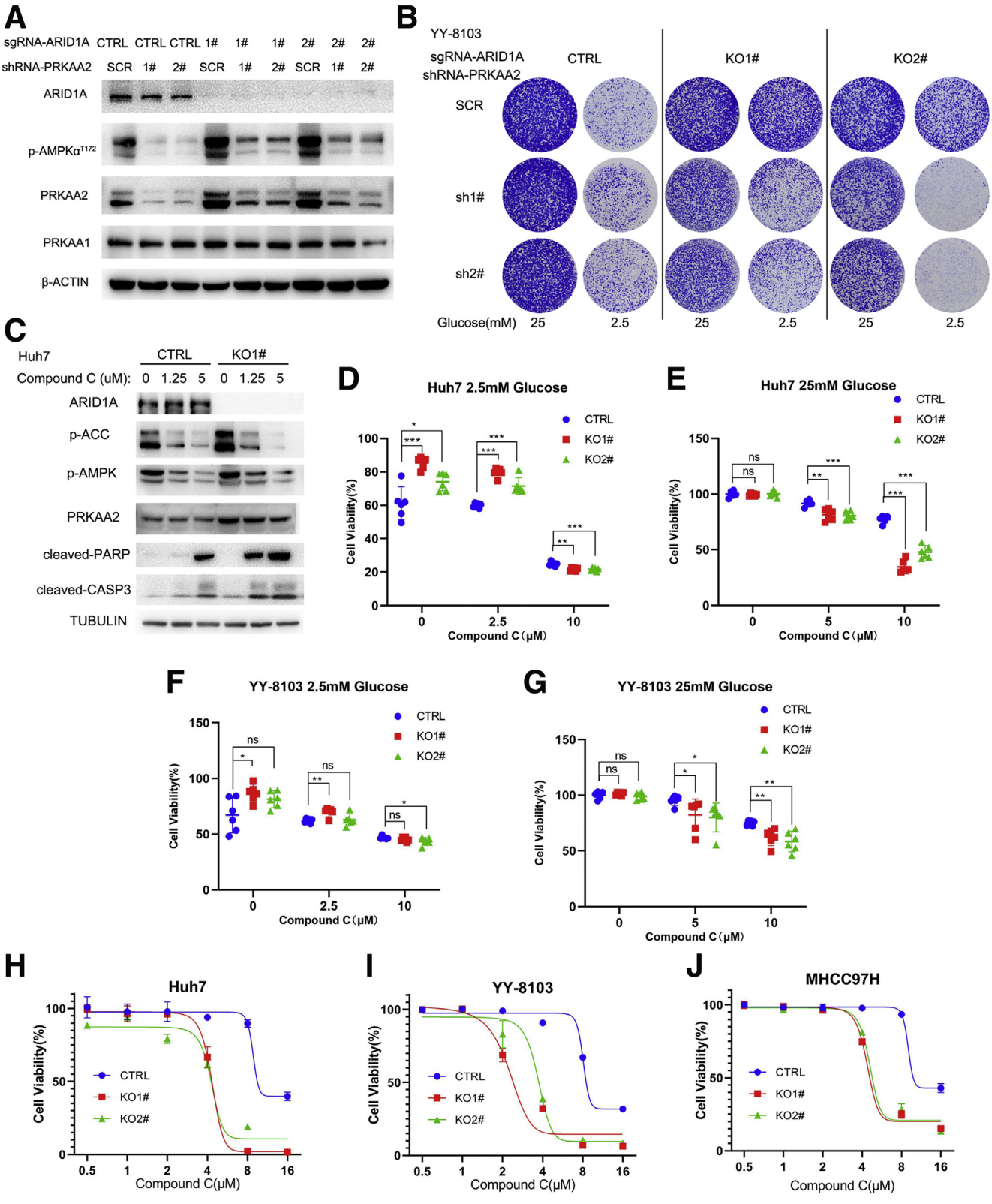
A
sgRNA-ARID1A CTRL CTRL CTRL 1# 1# 1# 2# 2# 2#
shRNA-PRKAA2 SCR 1# 2# SCR 1# 2# SCR 1# 2#
ARID1A
p-AMPKα(T172)
PRKAA2
PRKAA1
β-ACTIN
B
YY-8103
sgRNA-ARID1A
shRNA-PRKAA2
CTRL
KO1#
KO2#
SCR
sh1#
sh2#
Glucose(mM) 25 2.5 25 2.5 25 2.5
C
Huh7
CTRL
KO1#
Compound C (uM): 0 1.25 5 0 1.25 5
ARID1A
p-ACC
p-AMPK
PRKAA2
cleaved-PARP
cleaved-CASP3
TUBULIN
D
Huh7 2.5mM Glucose
CTRL
KO1#
KO2#
Cell Viability(%)
Compound C（μM）
E
Huh7 25mM Glucose
F
YY-8103 2.5mM Glucose
G
YY-8103 25mM Glucose
H
Huh7
I
YY-8103
J
MHCC97H
Compound C(μM)

ARID1A Regulates the Transcription of USP9X *by Recruiting HDAC1*

Consistent with data from the Gene Transcription Regulation Database (Figure 10*A*) and the ENCODE website (Figure 10*B*), ARID1A could bind to the *USP9X* promotor (Figure 10*C*). We analyzed the potential binding sites of HDAC1 in the *USP9X* promoter region from the hTFtarget website, and designed 4 pairs of chromatin immunoprecipitation (ChIP)-quantitative polymerase chain reaction (PCR) primers for verification (Figure 10*D*). We found that both ARID1A and HDAC1 binding sites were in proximity to site 4 (Figure 10*E*). To identify the involvement of HDAC1 in the regulation of *USP9X*, we treated cells with the HDAC1 inhibitor trichostatin A and panobinostat. In accordance with the previous study,[34] these inhibitors increased the protein level of *USP9X* (Figure 10*F*).

HDAC1 can deacetylate histone H3 at K9 and K27,[35] thus we examined the influence of AIRD1A on the acetylation of H3K9 and H3K27 at the *USP9X* promoter. Antibodies of Flag, ARID1A, HDAC1, ac-H3K9, and ac-H3K27 were used, respectively, for ChIP experiments and subsequent verification in control, ARID1A knockout Huh7/YY-8103 cells and ARID1A-WT/ARID1A-1989*-overexpressing PVTT/HEK293T cells. Knockout of ARID1A reduced the binding of HDAC1 and enhanced H3K9 and H3K27 acetylation (Figure 10*G* and *H*). In contrast, overexpression of ARID1A–WT increased the binding of HDAC1 and decreased H3K9 and H3K27 acetylation (Figure 10*I* and *J*). Although ARID1A-1989* could still bind to the *USP9X* promoter, it lost the ability to recruit HDAC1 to the promoter region of *USP9X* and could not affect H3K9/H3K27 acetylation (Figure 10*I* and *J*).

ARID1A Expression Negatively Correlates With USP9X/PRKAA2 and Influences HCC Patients' Survival

To further identify the correlation between ARID1A, PRKAA2, and USP9X, we examined their expression in clinical HCC samples by Western blot. As shown in Figure 11*A*, the protein level of ARID1A in HCC samples was negatively correlated with USP9X and PRKAA2. In addition, we used the Human Protein Atlas website, a large database of human proteins to analyze their relationship. There was indeed a negative correlation between ARID1A and USP9X/PRKAA2, despite the small sample size (Figure 11*B*). The aforementioned TMA was also used and stained with USP9X and PRKAA2 antibody and then scored by Vectra. USP9X showed a strong positive correlation with PRKAA2 (Figure 11*C* and *D*), while ARID1A had a negative correlation with USP9X (Figure 11*C* and *E*) and PRKAA2 (Figure 11*C* and *G*) in the 243 HCC samples. More importantly, patients in the ARID1A^{high}USP9X^{low} group had the longest overall survival time, while patients in the ARID1A^{low}USP9X^{high} group had the shortest overall survival time (Figure 11*F*). The ARID1A^{high}PRKAA2^{low} group and the ARID1A^{low}PRKAA2^{high} group showed similar trends (Figure 11*H*). These data highlight the clinical significance of the ARID1A/USP9X/PRKAA2 axis in HCC.

Potential Targeted Therapeutic Strategy for ARID1A-Deficient HCC

The clinical correlation between ARID1A, USP9X, and PKRAA2 promoted us to test the synthetic lethality between AMPK inhibition and ARID1A deficiency in vivo. In a subcutaneous tumor model of Huh7 (Figure 12*A*–*C*) and MHCC97H (Figure 12*D* and *E*) cells, the tumors in the ARID1A KO group were more sensitive to the inhibition by Compound C, although this inhibitor showed a modest effect on WT HCC cells. Consistently, phosphorylation and activity of AMPKα was significantly inhibited by the treatment of Compound C (Figure 12*F*). Immunohistochemical staining of cleaved-caspase 3 (Figure 12*G*) in tumor xenografts showed that ARID1A KO tumors treated with Compound C had increased apoptosis when compared with vehicle control and WT tumors. In addition, a luciferase-labeled orthotopic model of HCC was also used. After a month of Compound C administration, the fluorescence signals in the ARID1A KO group gradually diminished, while the fluorescence of the control group remained much stronger than that of ARID1A KO group (Figure 12*H* and *I*). More importantly, Compound C administration significantly prolonged the survival of tumor-bearing mice in ARID1A KO group (Figure 12*J*). Altogether, the in vitro and in vivo study verified the mechanism and indicated the therapeutic potential of Compound C for ARID1A-deficient HCC (Figure 12*K*).

Discussion

Although ARID1A was considered as a tumor suppressor in multiple cancers because of its high mutation rates, its role in HCC remains elusive. It was reported that ARID1A had a context-specific role in liver cancer, in which increased ARID1A promoted tumor initiation through CYP450-mediated oxidative stress, whereas reduced ARID1A increased metastasis owing to inhibition of relevant metastasis genes.[15] In the study conducted by Hu et al,[13] they found that ARID1A deficiency promoted

Figure 5. (***See previous page***). **ARID1A deletion maintains HCC cell survival in low-glucose conditions through activation of the AMPK pathway.** (*A*) Western blot analysis examining the knockdown efficiency of PRKAA2 and KO efficiency of ARID1A in YY-8103 cells. (*B*) The crystal violet assay examining the effects of PRKAA2 and ARID1A on colony-formation ability of YY-8103 cells under glucose deprivation. (*C*) Compound C treatment inhibits the AMPK signaling pathway. Cell viability of (*D* and *E*) control and ARID1A KO Huh7 and (*F* and *G*) YY-8103 cells treated with different doses of Compound C for 48 hours under low-glucose (2.5 mmol/L) or normal (25 mmol/L) condition is detected by cell counting kit-8 (CCK8) assay. Cell viability of (*H*) control and ARID1A knockout Huh7 cells, (*I*) YY-8103 cells, and (*J*) MHCC97H cells treated with Compound C for 72 hours is examined by CCK8 assay. Data are presented as means ± SD, n = 6 biologically independent samples, representative of 3 independent experiments. CTRL, control; SCR, scramble; sgRNA, single guide RNA. *$P<0.05$,**$P<0.01$,***$P<0.001$, ns, not significant.

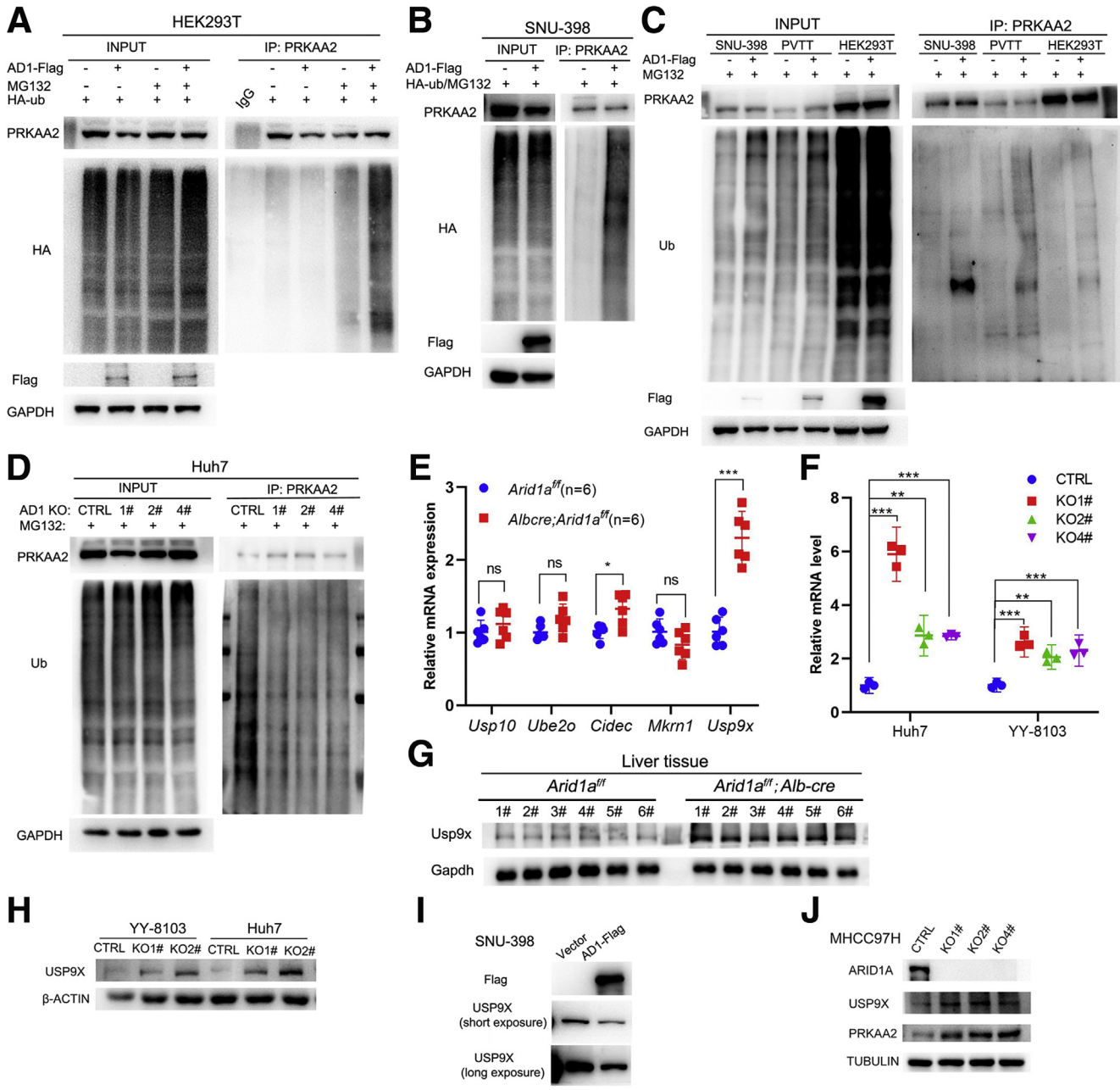

Figure 6. ARID1A regulates the ubiquitination of PRKAA2 through USP9X. The influence of ARID1A on the ubiquitination of PRKAA2 in (*A*) HEK293T, (*B* and *C*) SNU-398, PVTT, and (*D*) Huh7 cells. (*E*) The mRNA level of proteins involved in PRKAA2 ubiquitination or deubiquitination in liver tissues from control and *Arid1a* liver-specific knockout mice. (*F*) The mRNA level of *USP9X* in control and ARID1A KO Huh7 (*left*) and YY-8103 (*right*) cells is examined by real-time PCR. (*G*) Usp9x expression in liver tissues from control and *Arid1a* liver-specific knockout mice is examined by Western blot. (*H*) USP9X expression in control and ARID1A KO Huh7 and YY-8103 cell is examined by Western blot. (*I*) USP9X expression in control and ARID1A-overexpressing SNU-398 cells is examined by Western blot. (*J*) USP9X and PRKAA2 expressions in control and ARID1A KO MHCC97H cells are examined by Western blot. CTRL, control; GAPDH, glyceraldehyde-3-phosphate dehydrogenase. $^{*}P<0.05$,$^{**}P<0.01$,$^{***}P<0.001$, ns, not significant.

angiopoietin 2 (Ang2)-dependent tumor angiogenesis and tumor progression. In our study, ARID1A KO did not affect growth of HCC cells in normal condition. However, ARID1A KO cells showed survival advance upon glucose deprivation, whereas ARID1A-overexpressing cells were more vulnerable in low-glucose condition. Cellular starvation is typical in solid tumor as tumor cells outgrow the local vasculature.[36] Cells react to nutrient deprivation by adapting their metabolism, or, if starvation is prolonged, it can result in cell death. Our study suggested the role of ARID1A in regulating the adaptation of tumor cells to poor glucose supply, which facilitate their survival. Glucose starvation was reported to be associated with drug resistance.[37] It is interesting to investigate whether ARID1A

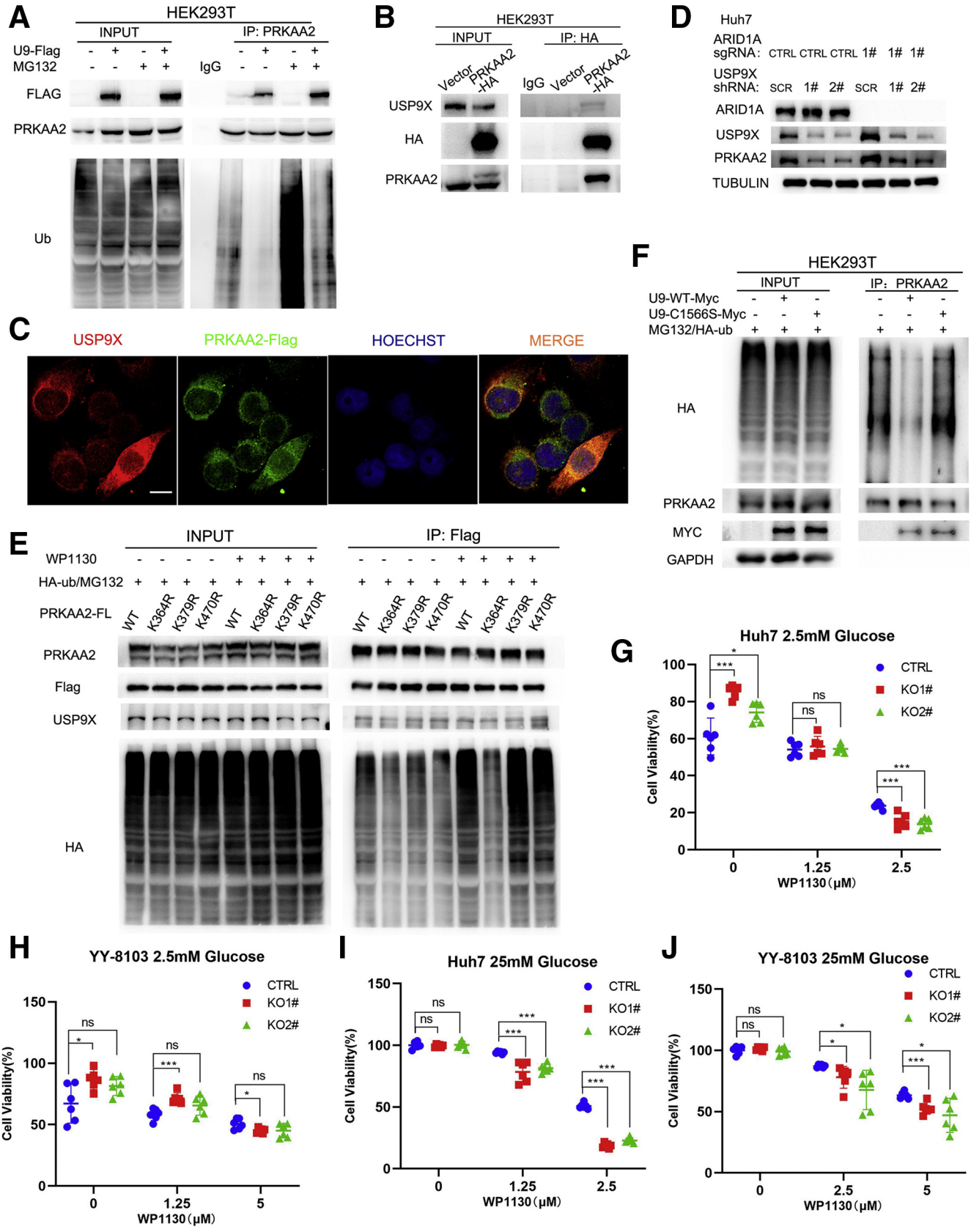
A
HEK293T
INPUT
IP: PRKAA2
U9-Flag
MG132
IgG
FLAG
PRKAA2
Ub
B
HEK293T
INPUT
IP: HA
Vector
PRKAA2 -HA
IgG
USP9X
HA
PRKAA2
D
Huh7
ARID1A sgRNA: CTRL CTRL CTRL 1# 1# 1#
USP9X shRNA: SCR 1# 2# SCR 1# 2#
ARID1A
USP9X
PRKAA2
TUBULIN
C
USP9X
PRKAA2-Flag
HOECHST
MERGE
F
HEK293T
INPUT
IP: PRKAA2
U9-WT-Myc
U9-C1566S-Myc
MG132/HA-ub
HA
PRKAA2
MYC
GAPDH
E
INPUT
IP: Flag
WP1130
HA-ub/MG132
PRKAA2-FL
WT
K364R
K379R
K470R
PRKAA2
Flag
USP9X
HA
G
Huh7 2.5mM Glucose
CTRL
KO1#
KO2#
Cell Viability(%)
WP1130(μM)
H
YY-8103 2.5mM Glucose
I
Huh7 25mM Glucose
J
YY-8103 25mM Glucose

deficiency–assisted adaptation to glucose starvation is associated with drug resistance, which may contribute to rapid relapse.

AMPK is well known for its role in nutrient sensing, and is induced by glucose deprivation.[38] Our study not only demonstrated that AMPK mediated ARID1A-regulated adaptation to glucose starvation, but also disclosed the role of the ARID1A/USP9X/AMPK axis in this event. Although several E3 ligases and deubiquitinases of AMPK have been reported, including ubiquitin-specific peptidase 10,[27] melanoma-associated antigen A3/6 (MAGE-A3/6), Tripartite Motif Containing 28 (TRIM28),[39] and glucose induced degradation deficient (GID) ubiquitin ligase complex,[40] here we reported a novel deubiquitinase, USP9X. USP9X was involved in AMPK activation during lysosomal damage.[41,42] However, in previous studies, the substrate of USP9X was Transforming growth factor beta-activated kinase 1 (TAK1), an upstream kinase and activator of AMPK. In our study, we identified USP9X as a novel deubiquitinase of PRKAA2 based on the following evidence: (1) USP9X interacted with PRKAA2; (2) USP9X significantly reduced the ubiquitination of PRKAA2; and (3) a loss-of-function mutant of USP9X as well as USP9X inhibitor WP1130 abolished its deuibiquitinating activity on PRKAA2. Furthermore, we identified K364 as the deubiquitination site on PRKAA2 for USP9X. In addition, we clarified the mechanism underlying the regulation of USP9X by ARID1A. We showed that ARID1A recruited HDAC1 to the promoter of *USP9X* via the C-terminal DUF3518 region. A hotspot mutant ARID1A-1989* lost this ability and could not regulate the transcription of USP9X. Furthermore, as a member of the SWI/SNF complex, ARID1A participates in the arrangement of the nucleosome landscape, which also was observed in our study (Figure 13). ARID1A overexpression and KO exerted different influences on nucleosome occupancy on the *USP9X* promoter. The role of ARID1A in the integrated regulation of nucleosome occupancy, histone acetylation, and gene transcription may be context-dependent and needs further investigation.

Because of the high mutation rates of ARID1A in cancer, there are considerable interests in developing targeted therapeutics for ARID1A-mutated cancers. The targets include the molecules showing mutual exclusivity with ARID1A, such as ARID1B and p53, and the molecules showing synthetic lethality with ARID1A mutation, such as ATR serine/threonine kinase (ATR),[43] aurora kinase A (AURKA),[16] poly(ADP-ribose) polymerase (PARP),[9] and enhancer of zeste 2 polycomb repressive complex 2 subunit (EZH2).[12] The current study identified a novel synthetic lethal partner of ARID1A mutation, the USP9X/AMPK axis. Either AMPK inhibitor Compound C or USP9X inhibitor WP1130 effectively suppressed the viability of ARID1A-deficient HCC cells in vitro, and the former also functioned in vivo. It is interesting to see whether the inactivation of USP9X and PRKAA2 could generally inhibit HCC cell growth. To address this issue, we examined the effect of shRNAs targeting PRKAA2 and PRKAA2/USP9X inhibitors on HCC cell growth under both normal and glucose-deprived conditions. We found that inactivation of PRKAA2/USP9X showed little effect in normal condition, and slightly enhanced cell death in the absence of glucose (Figure 14). We speculated that targeting the USP9X/PRKAA2 axis may be more effective for ARID1A-deficient HCC. Because Compound C was reported to inhibit cell growth in several cancers,[21,44–46] it may serve as a therapeutic candidate for ARID1A-deficient HCC.

In conclusion, our study has shown a novel function of ARID1A in HCC, and disclosed the role of the ARID1A/USP9X/AMPK axis in ARID1A-regulated cancer cell adaptation to low-glucose condition. We also provided synthetic lethal targets and potential therapeutic agents for ARID1A-deficient HCC, which may help improve the clinical outcome of these patients.

Materials and Methods

Cell Culture

The PVTT cell line was established in our laboratory, detailed information has been described previously. HEK293T cell and other human HCC cell lines used in this study were purchased from the Cell Bank of Type Culture Collection of Chinese Academy of Sciences, Shanghai Institute of Cell Biology, Chinese Academy of Sciences. All of these cells including the following primary hepatocytes were cultured in Dulbecco's modified Eagle medium (Gibco, Brooklyn, NY) containing 10% fetal bovine serum (Anlite), 100 U/mL penicillin (Sangon Biotech, Shanghai, China), and 100 U/mL streptomycin (Sangon Biotech, Shanghai, China). All of these cells were incubated at 37°C in a 5% CO_2 atmosphere with 21% oxygen and routinely checked for mycoplasma contamination, and cells used in this study were negative for mycoplasma.

Genetic Mouse Model

Alb-Cre mice were obtained from Jackson Laboratory (Sacramento, CA) and *Arid1a*$^{flox/flox}$ mice were kindly provided by Bin Zhou's laboratory (Shanghai Institute of Biochemistry and Cell Biology, Chinese Academy of Sciences,

Figure 7. (***See previous page***). **ARID1A regulates the stability of PRKAA2 through USP9X.** (*A*) Influence of USP9X on PRKAA2 ubiquitination in HEK293T cells. (*B*) Interaction between USP9X and PRKAA2 is examined by co-IP. (*C*) Localization of USP9X and PRKAA2 proteins in YY-8103 cells is examined by immunofluorescence assay. *Scale bar*: 25 μm. (*D*) Knockdown of USP9X inhibits the expression of PRKAA2 in Huh7 cells. (*E*) Ubiquitination of WT and 3 different PRKAA2 mutants upon WP1130 treatment in HEK293T cells. (*F*) Influence of USP9X-WT or USP9X-C1556S on the ubiquitination of PRKAA2 in HEK293T cells. (*G* and *H*) Cell viability of control, ARID1A KO Huh7, and YY-8103 cells treated with different doses of WP1130 under low-glucose condition for 48 hours. (*I* and *J*) Cell viability of control, ARID1A KO Huh7, and YY-8103 cells treated with different doses WP1130 under normal condition for 48 hours. CTRL, control; GAPDH, glyceraldehyde-3-phosphate dehydrogenase. *$P<0.05$, ***$P<0.001$, ns, not significant.

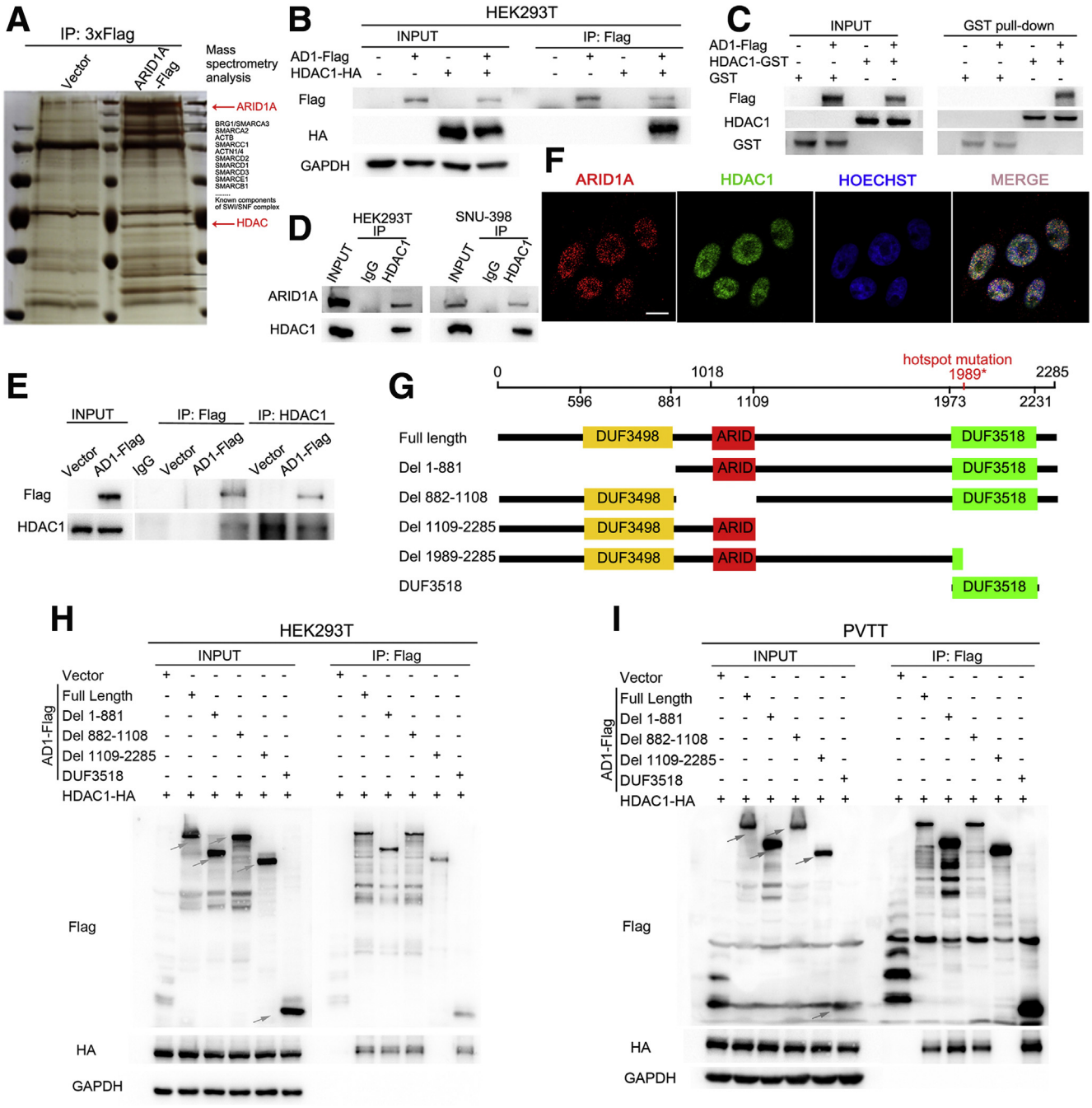

Figure 8. ARID1A interacts with HDAC1 through its C-terminal domain. (*A*) Silver-stained gel shows differential bands between control and ARID1A-overexpressing samples. (*B*) HEK293T cells were transfected with ARID1A-Flag and HDAC1-HA, and their interaction is examined by co-IP. (*C*) Interaction between ARID1A and HDAC1 is examined by GST pull-down. (*D*) The interaction between endogenous ARID1A and HDAC1 is examined by co-IP with HDAC1 antibody in HEK293T and SNU-398 cells. (*E*) The semi-exogenous interaction between ARID1A and HDAC1 is examined by co-IP with Flag antibody or HDAC1 antibody in HEK293T cells transfected with ARID1A-Flag. (*F*) Localization of ARID1A and HDAC1 proteins in YY-8103 cells is examined by immunofluorescence assay. *Scale bar*: 25 μm. (*G*) The schematic diagram of full-length ARID1A and 5 truncated mutants. (*H*) Interactions between different ARID1A mutants with HDAC1 in HEK293T cells are examined by co-IP with HA antibody. The *arrows* indicate exogenous ARID1A with Flag tag. (*I*) Interactions between different mutants of ARID1A and HDAC1 in PVTT cells are examined by co-IP with Flag antibody. The *arrows* indicate exogenous Flag-tagged ARID1A. DEL,deletion; GAPDH, glyceraldehyde-3-phosphate dehydrogenase.

Shanghai, China), *Arid1a* liver-specific knockout mice were generated by crossing *Alb-Cre* mice with *Arid1a*$^{flox/flox}$ mice. Primers for validation of genotypes are listed in Table 2. All mice were male in a C57BL/6 background and all animal experiments were performed under the approval of the Institutional Animal Care and Use Committee.

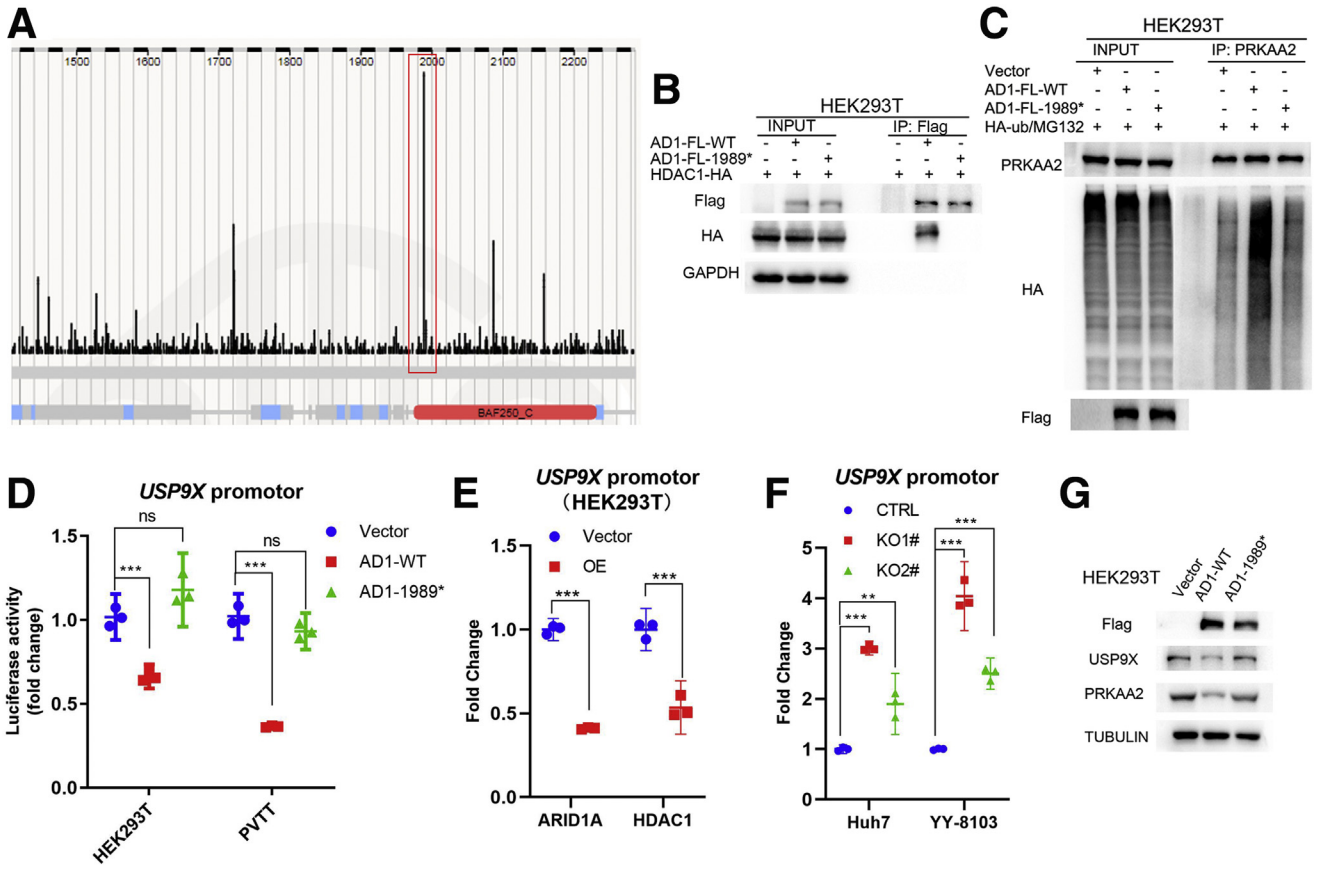

Figure 9. ARID1A regulates the promoter activity of *USP9X* via HDAC1. (*A*) Data from the Catalogue of Somatic Mutations in Cancer shows that 1989* is the most frequent mutation of ARID1A. (*B*) Interaction between ARID1A-WT or ARID1A-1989* mutation with HDAC1. (*C*) Influence of ARID1A-WT or ARID1A-1989* mutation on the ubiquitination of PRKAA2. (*D*) Influence of ARID1A-WT or ARID1A-1989* mutation on the promoter activity of *USP9X*. The promoter activity of *USP9X* in (*E*) HEK293T cells overexpressing ARID1A or HDAC1 (OE) or in (*F*) ARID1A knockout Huh7 and YY-8103 cells is examined by luciferase reporter assay. (*G*) Influence of ARID1A-WT or ARID1A-1989* mutation on the expression of USP9X and PRKAA2. CTRL, control; GAPDH, glyceraldehyde-3-phosphate dehydrogenase. $^{**}P<0.01$, $^{***}P<0.001$, ns, not significant.

Primary Hepatocyte Isolation

Primary hepatocytes from mice were isolated as follows: 10-week-old mice were anesthetized with chloral hydrate, and then the liver was exposed when the abdominal skin was cut off carefully. The needle was inserted carefully from the inferior vena cava, and then the hepatic portal vein was cut off. The liver was washed with buffer 1 (4.8 mmol/L KCl, 1.2 mmol/L $MgSO_4$, 1.2 mmol/L KH_2PO_4, 120 mmol/L NaCl, 24 mmol/L $NaHCO_3$, 20 mmol/L glucose, 5 mmol/L HEPES, and 0.1 mmol/L EGTA [pH = 7.4]) at a speed of 25 m/s until the liver color remained unchanged for approximately 3 minutes. Then, it was digested with buffer 2 (4.8 mmol/L KCl, 1.2 mmol/L $MgSO_4$, 1.2 mmol/L KH_2PO_4, 120 mmol/L NaCl, 24 mmol/L $NaHCO_3$, 20 mmol/L glucose, 5 mmol/L HEPES, and 1.37 mmol/L $CaCl_2$ [pH = 7.4]) containing 8000 U collagenase for approximately 20 minutes at a flow rate of 18 m/s. Carefully peel out the digested liver with scissors, cut them into 1 mm^3 size, gently blow the digested liver tissue pieces evenly, and then filter the separated cells from the 70-μm diameter filter membrane. Place the separated cells into a 4ºC centrifuge at 800 *g* for 3 minutes, pour out the supernatant, and add 3 mL serum-free medium. Then, add 4.38 mL Percoll solution and 0.62 mL 10× phosphate-buffered saline (PBS). After fully mixing, centrifugation at 4ºC for 10 minutes at 800 *g*, the precipitated fraction is the primary living liver cells. Washed the precipitates with serum-free medium, and then plated the cells into the 6-well plate at the density of of 5×10^5 cells/well. It should be noted that the 6-well plate needs to be coated with collagen in advance.

HCC Samples

All HCC samples including TMAs were obtained from Eastern Hepatobiliary Surgery Hospital, Second Military Medical University (Shanghai, China). Human HCC samples were frozen in liquid nitrogen immediately after surgery. All experiments were approved by the Ethical Committee of Shanghai Institutes for Biological Sciences, Chinese Academy of Sciences (Shanghai, China) following the Declaration of Helsinki ethical guidelines.

Plasmids and Stable Cell Lines

Coding sequence of *ARID1A*, *PRKAA2*, *USP9X*, and *HDAC1* were inserted in to pHAGE-fEF1a-IRES-ZsGreen or pCDNA3 with tags such as Flag, Myc, or HA for transient expression. In addition, mutations of *ARID1A* (*del 1-881*, *del 882-1108*, *del 1109-2285*, *del 1989-2285*, *DUF3518*), *PRKAA2* (*K364R*, *K379R*, *K470R*), and *USP9X* (*C1566S*) were constructed. The promoter of *USP9X* was cloned from genome of HEK293T

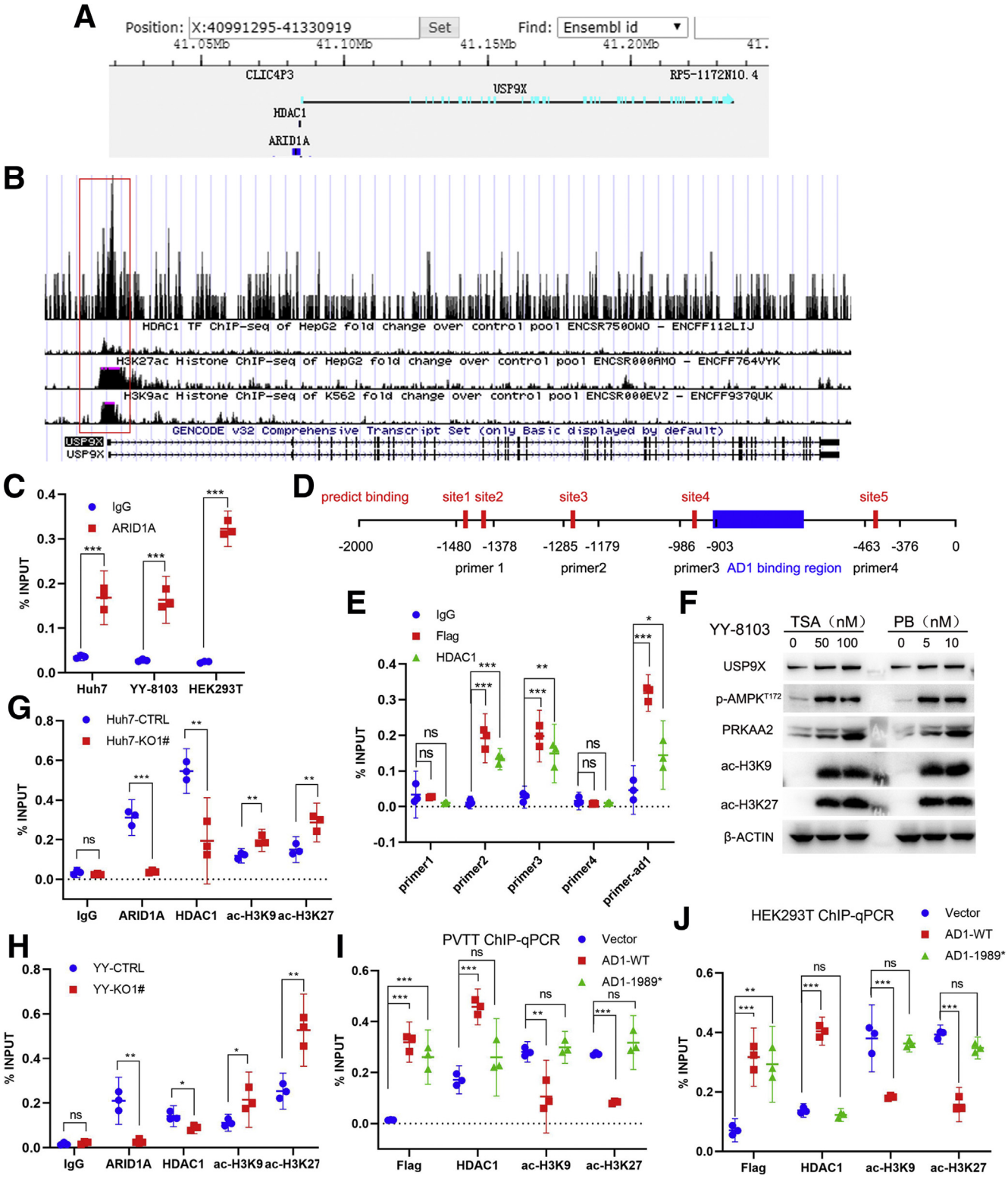

and inserted in pGL3-Basic plasmid. For the GST pull-down experiment, the coding sequence of *HDAC1* was inserted in pGEX4T-1 plasmid. Primers for gene cloning are listed in Table 3. pLKO.1-puro was used to produce shRNA lentivirus of *PRKAA2*. LentiCRISPRv2-puro was used to produce Cas9-mediated gene KO lentivirus of *ARID1A*. Primers for shRNA and (single guide RNA (sgRNA) are listed Table 4. For stable cell line production, HCC cell lines were transfected with corresponding lentivirus, followed by cell selection by green fluorescent protein (GFP) sorting (pHAGE-fEF1a-IRES-ZsGreen) or puromycin treatment (pLKO.1-puro and LentiCRISPRv2-puro). The *USP9X* complementary DNA was kindly provided by Yong-Jun Dang (School of Basic Medical Sciences, Fudan University, Shanghai, China). Lentivirus packaging is described in detail later.

Lentivirus Packaging

The lentiviruses were packaged in HEK293T cells and harvested under the following conditions: 20,000 rpm at 4ºC for 2 hours. In detail, when HEK293T cells grew to 80% density, transient transfection of the mix plasmids (core plasmid:PSPAX:PMD2G = 12 μg:9 μg:3 μg) was performed by calcium chloride reagent, and, after 24 hours, the supernatant was removed and fresh medium was added. Only the supernatant suspensions of 48 and 72 hours was kept. The collected liquid was filtered with a 0.22-μm filter membrane, and then 5 mL of 20% sucrose solution was added. The supernatant was centrifuged at 4ºC and 20,000 rpm for 2 hours. The supernatant was poured out and the residue was carefully removed. Serum-free medium (1 mL) was added for dissolution. The packaged lentivirus could be used for subsequent cell infection experiments.

Cell-Derived Xenograft

Subcutaneous tumorigenesis. Five-week-old male nude mice were divided randomly into 4 groups (n = 6 per group) and injected subcutaneously with Huh7 or MHCC97H cells (2 groups for ARID1A-control (CTRL) and 2 groups for ARID1A-KO, $1x10^6$ cells per mouse) mixed with same volumes of BD Biocoat Matrigel (Corning Life Sciences, Tewksbury, MA). One week later, when the tumor grew to approximately 5 mm in diameter, Compound C or vehicle was delivered to the nude mice by intraperitoneal injection, with a dosage of 10 mg/kg every 2 days. During this time, tumor size was measured every day or every 2 days using digital Vernier calipers (Deli, Ningbo, Zhengjiang, China). When the tumor was big enough, the mice were killed and photographed. The tumor was taken out and weighed. The tumor volume was calculated as follows: $mm^3 = 0.5 \times length \times width^2$. These experiments were approved by the Institutional Animal Care and Use Committee, Shanghai Institutes for Biological Sciences, Chinese Academy of Sciences.

Orthotopic HCC model. Luciferase-labeled Huh7 cell lines (10^6 cells per mouse) mixed with 1/2 volumes of Matrigel were injected into the left lobe of livers of 5-week-old male nude mice (2 groups for ARID1A-CTRL and 2 groups for ARID1A-KO, n = 6 per group). A week after injection, both the control and KO groups were labeled with luciferase in the liver successfully, Compound C or vehicle was delivered to the nude mice by intraperitoneal injection, with a dosage of 10 mg/kg every 2 days for a total of 30 days. Every 10 days, Mice were injected intraperitoneally with D-luciferin, anesthetized by isoflurance, and photographed in IVIS system (Xenogen, Alameda, CA). For survival assay, the tumor-bearing mice, which were treated with Compound C or vehicle later, were fed normally until their death, the date of death and fluorescent signal were recorded.

RNA Isolation and Real-Time PCR

Total RNA from HCC and paired normal tissues was extracted with TRIzol reagent (Invitrogen,Carlsbad, CA) and 2 μg RNA was reverse transcribed into complementary DNA using the reverse-transcription kit (Promega, Madison, WI). The mRNA level of target genes was detected by the Thermo Scientific (Waltham, MA) detection system (PIKOREAL96) with 2×SYBR Green kit (Yeasen Biotech, Shanghai, China). The real-time PCR procedure was as follows: 40 cycles of 95°C for 20 seconds, 60°C for 30 seconds, followed by 72°C for 30 seconds, and then 72°C for 10 minutes. The primers used are listed in Table 5.

Western Blot and Co-IP

Culture medium was removed, and cells were washed twice with precooling of PBS (1.37 mol/L NaCl, 27 mmol/L KCl, 100 mmol/L Na_2HPO_4, 20 mmol/L KH_2PO_4 [pH = 7.4]). Cells were lysed with RIPA buffer (50 mmol/L Tris-HCl, 150 nmol/L NaCl, 0.5% sodium deoxycholate, 0.1% sodium dodecyl sulfate [SDS], 1% Nonidet P-40 [pH = 7.4]) containing protease inhibitors and phosphatase inhibitor (Selleck, Shanghai, China) to extract protein, and

Figure 10. (***See previous page***). **ARID1A regulates the transcription of *USP9X* via HDAC1.** Data from (*A*) GTAD or (*B*) ENCODE suggest that both ARID1A and HDAC1 can bind to the promoter region of *USP9X*. (*C*) The binding of ARID1A to *USP9X* promotor in Huh7, YY-8103, and HEK293T cells is measured by ChIP–quantitative PCR (qPCR) assay. (*D*) The diagram of *USP9X* promoter. The 5 red marked regions indicate predicted binding sites of HDAC1 in the promoter region of *USP9X*, with 4 pairs of primers listed below. The blue marked region indicates ARID1A binding region with primers named primer-ad1. (*E*) Primer 2, primer 3, and primer ad1 are better among the 5 primers tested in HEK293T by ChIP–qPCR. (*F*) The protein level of USP9X and PRKAA2 upon HDAC1 inhibitor trichostatin A (TSA) and panobinostat (PB) treatment. (*G* and *H*) The binding of ARID1A and HDAC1 to the *USP9X* promoter, and the level of ac-H3K9/H3K27 in the *USP9X* promoter in (*G*) control and ARID1A KO Huh7 cells and (*H*) YY-8103 cells is examined by the ChIP–qPCR assay. The binding of the indicated molecules (ARID1A-WT/ARID1A-1989*-Flag, HDAC1) to the *USP9X* promoter and the level of ac-H3K9/ac-H3K27 in (*I*) control, ARID1A-overexpressing PVTT cells and (*J*) HEK293T cells is examined by the ChIP–qPCR assay. CTRL, control. *$P<0.05$, **$P<0.01$, ***$P<0.001$, ns, not significant.

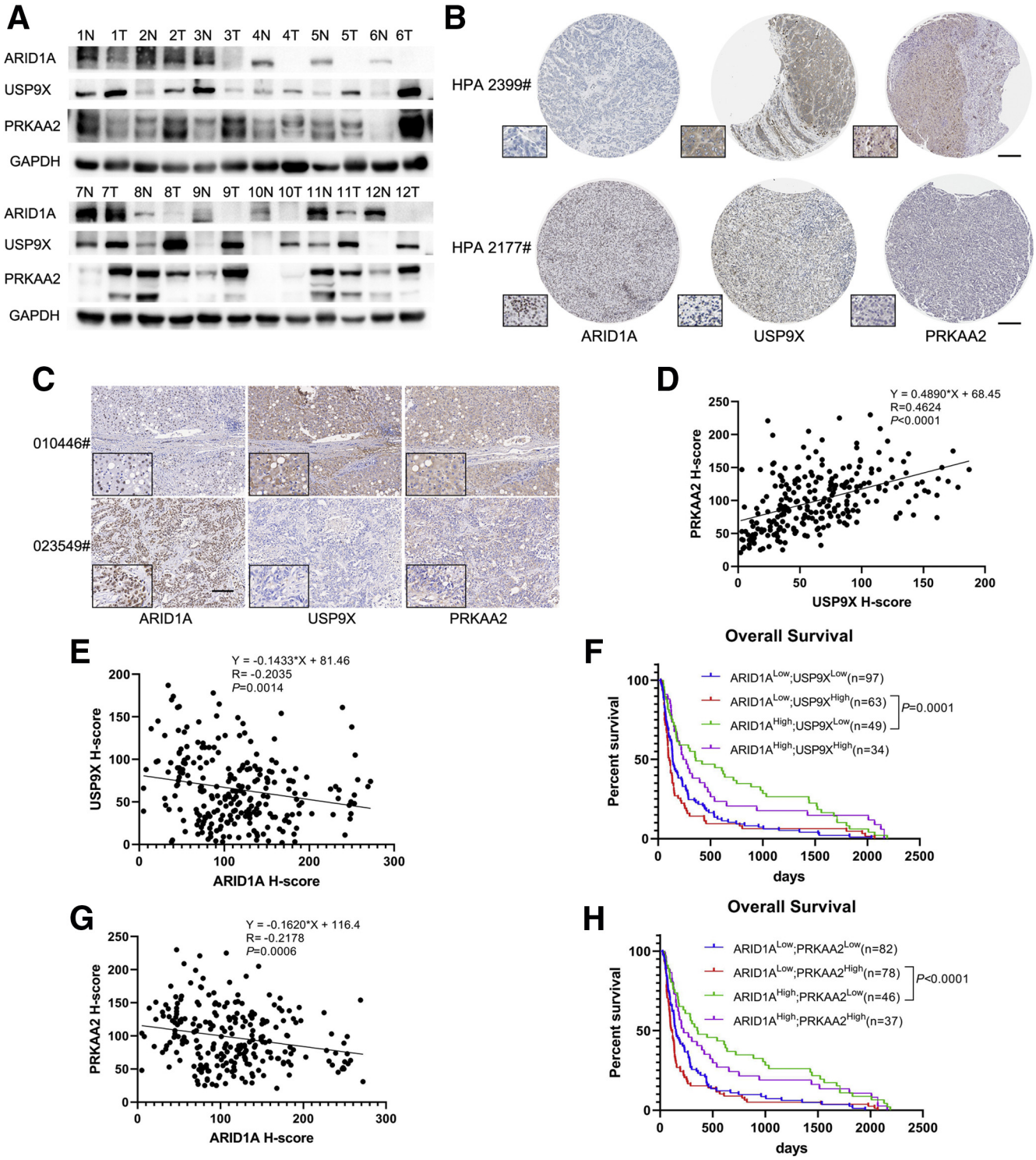

Figure 11. ARID1A negatively correlates with USP9X/PRKAA2 and influences HCC patients' survival. The correlation among ARID1A, USP9X, and PRKAA2 in the clinical samples is examined by (*A*) Western blot or by (*B*) immunohistochemical staining in the Human Protein Atlas (HPA) database. (*C*) Immunohistochemistry staining of ARID1A, USP9X, and PRKAA2 in HCC tissues in TMAs. *Scale bar*: 100 μm. (*D*) The correlation between USP9X and PRKAA2 at the protein level (N = 243) is analyzed using H-scores from TMA analysis. (*E*) The correlation between ARID1A and USP9X at the protein level (N = 243) is analyzed using H-scores from TMA analysis. (*F*) Comparison of overall survival between HCC patients with different ARID1A/USP9X expressions. Data are analyzed using the log-rank test. (*G*) The correlation between ARID1A and PRKAA2 at the protein level (N = 243) is analyzed using H-scores from TMA analysis. (*H*) Comparison of overall survival between HCC patients with different ARID1A/PRKAA2 expressions. GAPDH, glyceraldehyde-3-phosphate dehydrogenase.

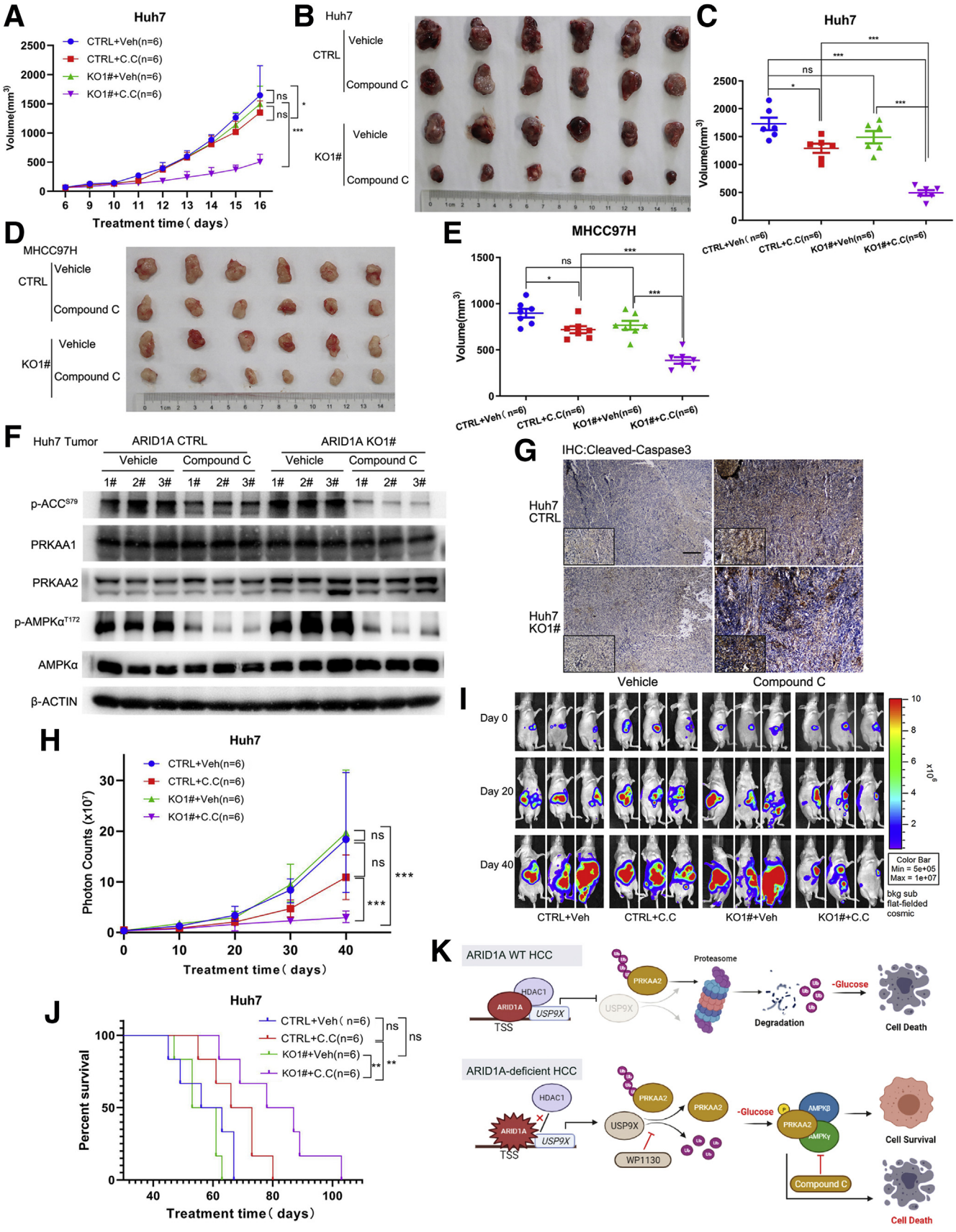
A
Huh7
CTRL+Veh(n=6)
CTRL+C.C(n=6)
KO1#+Veh(n=6)
KO1#+C.C(n=6)
Volume(mm3)
Treatment time（days）
ns
ns
*
***
B
Huh7
CTRL
Vehicle
Compound C
KO1#
Vehicle
Compound C
C
Huh7
Volume(mm3)
CTRL+Veh（n=6)
CTRL+C.C(n=6)
KO1#+Veh(n=6)
KO1#+C.C(n=6)
D
MHCC97H
CTRL
Vehicle
Compound C
KO1#
Vehicle
Compound C
E
MHCC97H
Volume(mm3)
F
Huh7 Tumor
ARID1A CTRL
ARID1A KO1#
Vehicle
Compound C
1# 2# 3# 1# 2# 3# 1# 2# 3# 1# 2# 3#
p-ACCS79
PRKAA1
PRKAA2
p-AMPKαT172
AMPKα
β-ACTIN
G
IHC:Cleaved-Caspase3
Huh7 CTRL
Huh7 KO1#
Vehicle
Compound C
H
Huh7
Photon Counts (x10^7)
Treatment time（days）
I
Day 0
Day 20
Day 40
CTRL+Veh
CTRL+C.C
KO1#+Veh
KO1#+C.C
Color Bar
Min = 5e+05
Max = 1e+07
bkg sub
flat-fielded
cosmic
J
Huh7
Percent survival
Treatment time（days）
K
ARID1A WT HCC
HDAC1
ARID1A
USP9X
TSS
PRKAA2
USP9X
Proteasome
Degradation
-Glucose
Cell Death
ARID1A-deficient HCC
WP1130
AMPKβ
AMPKγ
Compound C
Cell Survival
Cell Death

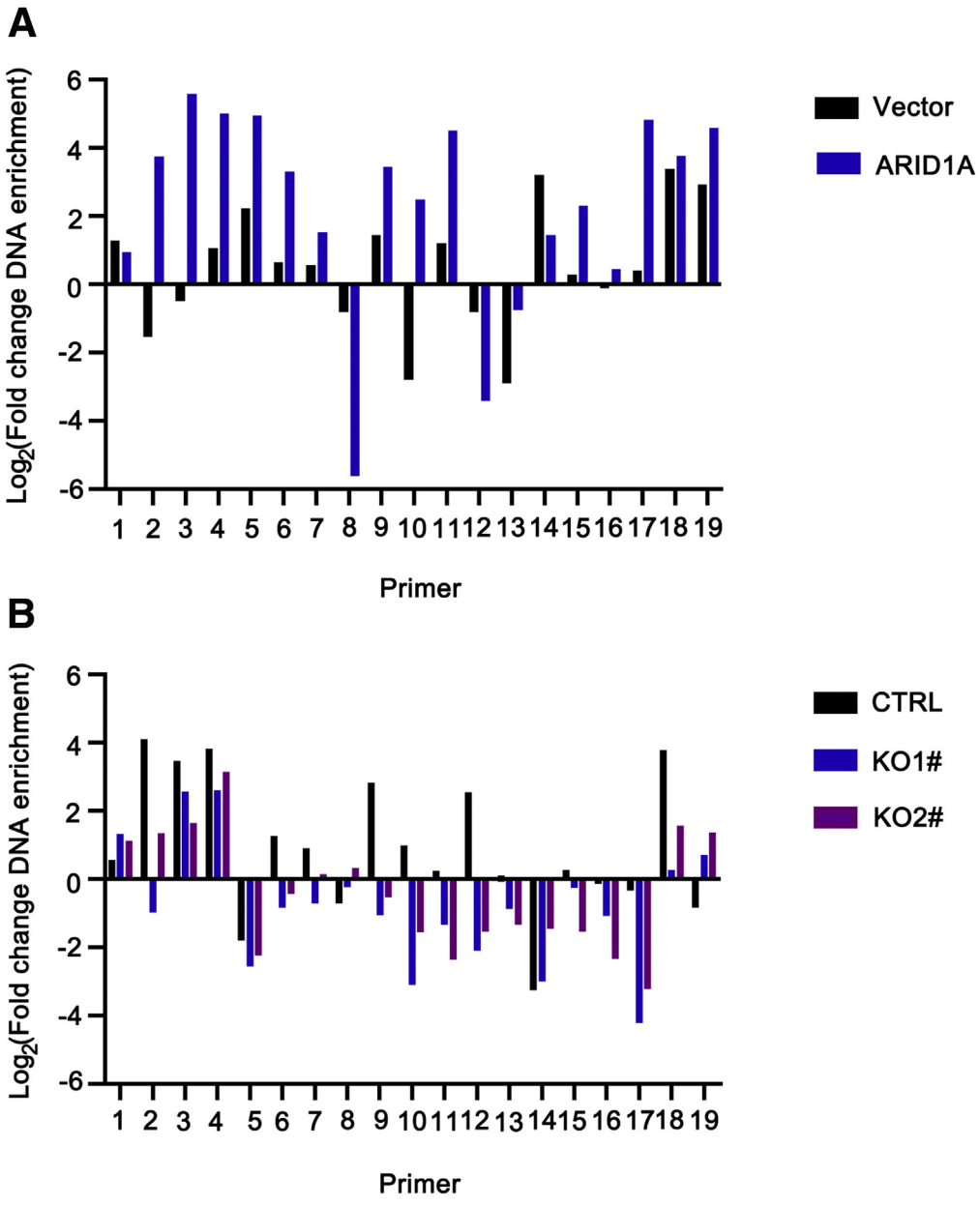

Figure 13. ARID1A influences nucleosome occupancy on the *USP9X* promoter. The nucleosome occupancy on the *USP9X* promoter in both (*A*) ARID1A-overexpressing cells and (*B*) KO cells is examined by a nucleosome scanning assay. CTRL, control.

then protein was quantified using Bradford reagent (Bio-Rad, Richmond, CA). After SDS–polyacrylamide gel electrophoresis separation, protein was transferred onto a polyvinylidene difluoride membrane, sealed with 5% (wt/vol) bovine serum albumin (BSA) for 1 hour, and then the corresponding first antibodies were added to incubate overnight at 4°C. The next day, horseradish peroxidase–conjugated secondary antibody of the corresponding species was added and incubated for an hour, and then detected by the Tanon 5200 automatic

Figure 12. (***See previous page***). **Potential targeted therapy for ARID1A-deficient HCC.** (*A*) The growth curves of subcutaneous tumors derived from control or ARID1A KO Huh7 cells in nude mice with administration of vehicle or Compound C. (*B*) Image of the tumors derived from control or ARID1A KO Huh7 cells in vehicle and Compound C groups at the end of the scheduled treatment. (*C*) Comparison of tumor size between different groups at the end of Compound C treatment (n = 6 for each group). (*D*) Image of the tumors derived from control or ARID1A knockout MHCC97H cells in vehicle and Compound C groups at the end of treatment. (*E*) Comparison of tumor size in panel *D* (n = 6 for each group). (*F* and *G*) Expression of the indicated molecules in tumor xenografts derived from control and ARID1A knockout Huh7 cells in different groups. *Scale bar*: 100 μm. (*H*) The total fluorescent signal of the tumors, (*I*) representative images, and (*J*) survival curve of the mice inoculated with either control or ARID1A KO Huh7 cells in the orthotopic model treated with vehicle or Compound C. (*K*) Schematic representation of the molecular mechanism of wild-type ARID1A and loss-of-function mutants. CTRL, control; Veh, vehicle. **P*<0.05, ***P*<0.01, ****P*<0.001, ns, not significant.

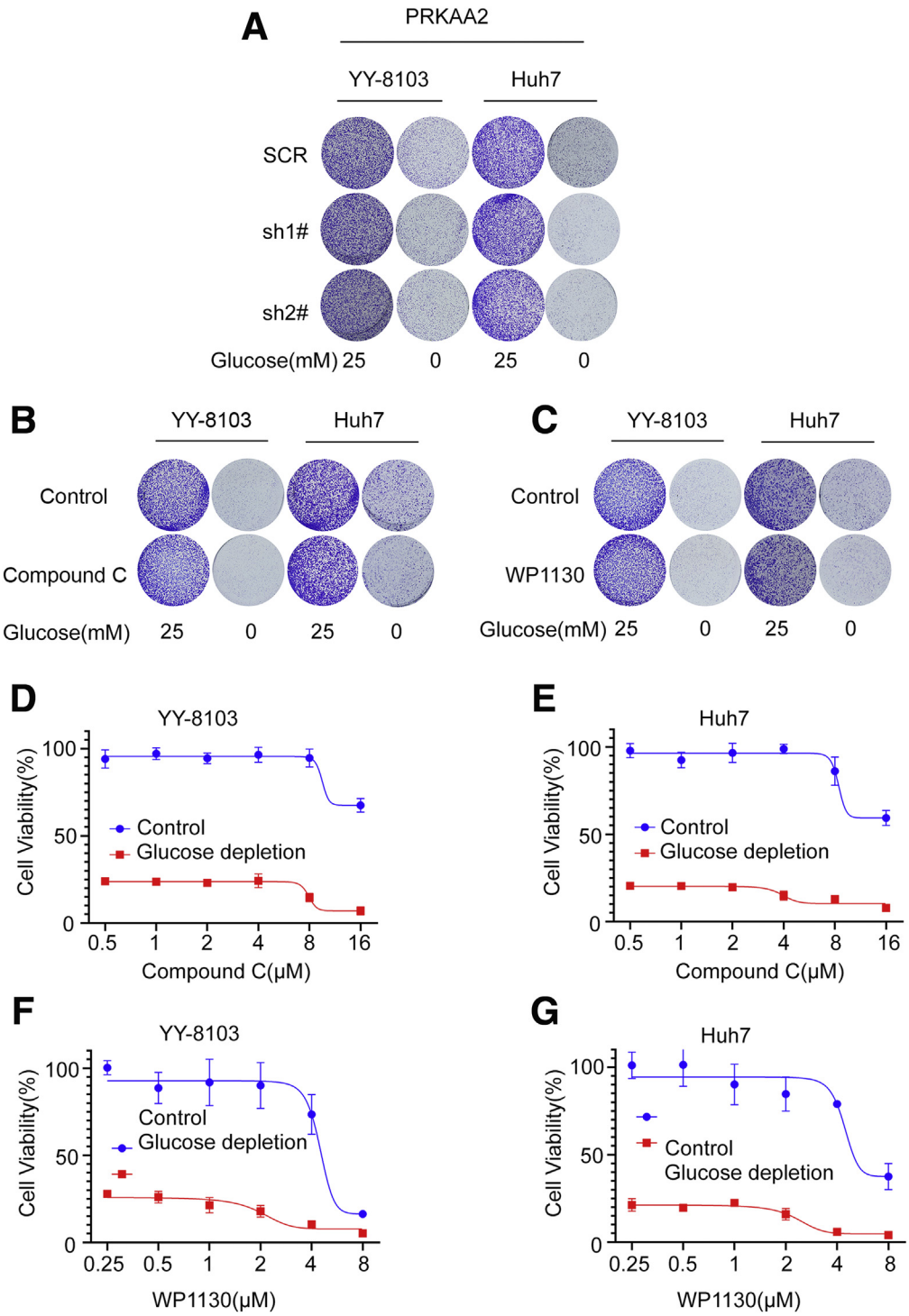

Figure 14. The effects of inactivation of PRKAA2 and USP9X on HCC cell growth. (*A*) The growth of control (Scramble, SCR) and PRKAA2 knockdown (sh1#, sh2#) cells is measured by crystal violet staining under both normal and glucose-deprived conditions. The influences of (*B*, *D*, *E*) Compound C and (*C*, *F*, *G*) WP1130 on HCC cell growth is measured by crystal violet staining or cell counting kit-8 (CCK8) assay under both normal and glucose-deprived conditions.

chemiluminescence imaging analysis system (Tanon, Shanghai, China). Tris-buffered saline (50 mmol/L Tris, 150 mmol/L NaCl, 1% Nonidet P-40, 1 mmol/L EDTA, 1 mmol/L Na_3VO_4, 10 mmol/L NaF, 2.5 mg/mL aprotinin, 10 mmol/L leupeptin, 1 mmol/L β-glycerophosphate, 4-(2-aminoethyl), 10 mmol/L benzenesulfonyl fluoride hydrochloride, and 10 mmol/L iodoacetate [pH = 7.4]) was used to lyse cells, and antibody against Flag, HA, or PRKAA2 was added into cell lysis to incubate overnight at 4ºC. The next day, ProteinA beads (17127901; Cytiva) or Protein G beads (17-0756-01; GE Healthcare, Waukesha, WI) were added to incubate for 3 hours. After washing 3 times with Tris-Buffered Saline (TBS) to remove nonspecific binding proteins, protein binding to beads was boiled with 2× loading buffer and examined by Western blot. Sliver staining was performed using the Beyotime (Haimen, Jiangsu, China) Fast Silver

Table 2. Primers for mouse genotyping

Primer	Sequence
Arid1a-flox	F: 5'-ATCCTGTGTACAGAACTTAAGC-3' R: 5'-CTTTCCCATTACTCTTTCCTGC-3'
Alb-cre	F: 5'-GAAGCAGAAGCTTAGGAAGATGG-3' R: 5'-TTGGCCCCTTACCATAACTG-3'

Stain Kit as its protocol. Differential bands were disposed with mass spectrometry analysis. Antibodies against acetyl–histone H3 (Lys9) (9649), acetyl–histone H3 (Lys9) (8173), ULK1 (8054), phospho-ULK1 (Ser317) (12753), phospho-ULK1 (Ser555) (5869), phospho-ULK1 (Ser757) (6888), acetyl-CoA carboxylase (3676), phospho-acetyl-CoA carboxylase (Ser79) (11818), AMPKα (2532), phospho-AMPKα (Thr172) (2535), LC3B (3868), and HDAC1 (34589) were purchased from Cell Signaling Technology (Danvers, MA); antibodies against PRKAA1 (10929), PRKAA2 (18167), USP9X (55054), glyceraldehyde-3-phosphate dehydrogenase (10494), and liver kinase B1 (10746) were purchased from Proteintech (Rosemont, IL); antibodies against ARID1A (sc-32761), α-tubulin (sc-32293), β-actin (sc-47778), ubiquitin (sc-8017), and c-myc (sc-764) were purchased from Santa Cruz Biotechnology (Dallas, Texas); and antibodies against Flag and HA were purchased from Sigma-Aldrich (St. Louis, MO).

Immunohistochemistry and Immunofluorescence

The tissue sections and tissue microarrays were fixed with formaldehyde, dehydrated with xylene, repaired with sodium citrate antigen, and then removed with hydrogen peroxide. Then, sections were blocked by 0.01 mol/L PBS supplemented with 3% BSA, 5% normal goat serum, and 0.3% Triton X-100 (Sangon Biotech, Shanghai, China). Next, sections were incubated with the first antibody overnight at 4°C. After washing 3 times with 0.01 mol/L PBS, sections were incubated with the secondary antibody for 2 hours and visualized with 3,3′-diaminobenzidine tetra hydrochloride using the 3,3′-Diaminobenzidine Tetra Hydrochloride Detection Kit (GK500710; Gene Tech). Next, sections were stained with hematoxylin. The extent and staining intensity of protein were further photographed and scored automatically by the Vectra 2 system. The outcome of staining was determined using the H-score, defined by the following equation: H-score = 100 ΣPi*I, where i indicates the staining intensity of the tumor cell with a score from 0 to 3, and Pi indicates the percentage of the stained tumor cells. For immunofluorescence, cells on slides were fixed with 4% formaldehyde, followed by blocking using 0.01 mol/L PBS supplemented with 3% BSA, 5% normal goat serum, and 0.3% Triton X-100, and then stained with the indicated primary antibodies and fluorescent secondary antibody (Alexa Fluor 488–conjugated donkey anti-rabbit IgG and Alexa Fluor 555–conjugated goat anti-rabbit IgG) and

Table 3. Primers for Gene Cloning

Primer	Sequence
ARID1A	F: 5'-AAGCTTCGATACTAGTATGGCCGCGCAGGTCGC-3' R: 5'-TCCCTCGAGATCTTAATTAATTACTTGTCATCGTCATCCTTGTAGTCGATGTCATG-3'
PRKAA2	F: 5'-GGGGTACCATGGCTGAGAAGCAGAAGCAC-3' R: 5'-GCTCTAGAACGGGCTAAAGTAGTAATCAGACTG-3'
USP9X	F: 5'-GGGGTACCATGACAGCCACGACTCGTGGCTC-3' R: 5'-GCTCTAGACATTGATCCTTGGTTTGAGGTGGGGATACTTC-3'
HDAC1	F: 5'-GGGGTACCATGGCGCAGACGCAGG-3' R: 5'-GCTCTAGACAGGCCAACTTGACCTCCTCCTTG-3'
ARID1A (del 1-881)	F: 5'-CTTGGTACCCCGGATCCCATCTAGAATGGGGATGTGTCCCCCACCAGGGGGCATGAAC-3' R: 5'-GTTCATGCCCCCTGGTGGGGGACACATCCCCATTCTAGATGGGATCCGGGGTACCAAG-3'
ARID1A (del 882-1108)	F: 5'-CAATATGCCACCTCAGGTTGGGTCAGGAGAAGACCCTCCCCCAGACATCTTTGCAG-3' R: 5'-CTGCAAAGATGTCTGGGGGAGGGTCTTCTCCTGACCCAACCTGAGGTGGCATATTG-3'
ARID1A (del 1109-2285)	F: 5'-GTCTCTATGCCTTTGAATGCAAGATTGAATCCTCGACGGACGCGTGGGACTACAAAGAC-3' R: 5'-GTCTTTGTAGTCCCACGCGTCCGTCGAGGATTCAATCTTGCATTCAAAGGCATAGAGAC-3'
ARID1A (del 1989-2285)	F: 5'-GCGCTGCGTCTGTGTGTCCAATACCATTTCGACGGACGCGTGGGACTACAAAGACCATG-3' R: 5'-CATGGTCTTTGTAGTCCCACGCGTCCGTCGAAATGGTATTGGACACACAGACGCAGCGC-3'
ARID1A (DUF3518)	F: 5'-GGGGTACCATGTCTCTTGCCAAGCGCTG-3' R: 5'-GCTCTAGACGCATCATGTCCACACTAGTTGG-3'
PRKAA2 (K364R)	F: 5'-TGCCATGCATATTCCCCCAGGCCTGAGACCTCATCCAGAAAGGATGCCACCTCT-3' R: 5'-AGAGGTGGCATCCTTTCTGGATGAGGTCTCAGGCCTGGGGGAATATGCATGGCA-3'
PRKAA2 (K379R)	F: 5'-ATGCCACCTCTTATAGCAGACAGCCCCAGAGCAAGATGTCCATTGGATGCACTGAATA-3' R: 5'-TATTCAGTGCATCCAATGGACATCTTGCTCTGGGGCTGTCTGCTATAAGAGGTGGCAT-3'
PRKAA2 (K470R)	F: 5'-TGATAACAGGAGCTATCTTTTGGACTTTAGAAGCATTGATGATGAAGTAGTGGAGCA-3' R: 5'-TGCTCCACTACTTCATCATCAATGCTTCTAAAGTCCAAAAGATAGCTCCTGTTATCA-3'
USP9X (C1566S)	F: 5'-GTGGGGCTGAAAAATGCCGGTGCTACTAGTTACATGAATTCTGTGATTCAGCAAC-3' R: 5'-GTTGCTGAATCACAGAATTCATGTAACTAGTAGCACCGGCATTTTTCAGCCCCAC-3'
USP9X promotor (-1852 ~ -161)	F: 5'-CAGCCTATAGTGTACGCGGG -3' R: 5'-GCCCAAGACCCGAAGTTCTC-3'

Table 4. Primers for shRNA or CRISPR/Cas9

Primer	Sequence
ARID1A sgRNA 1#	F: 5'-CACCGGTTGCCCAGGCTGCTGGCGG-3' R: 5'-AAACCCGCCAGCAGCCTGGGCAACC-3'
ARID1A sgRNA 2#	F: 5'-CACCGCGGGTTGCCCAGGCTGCTGG-3' R: 5'-AAACCCAGCAGCCTGGGCAACCCGC-3'
ARID1A sgRNA 4#	F: 5'-CACCGGTCTTCCACCAACAACATGG-3' R:5'-AAACCCATGTTGTTGGTGGAAGACC-3'
PRKAA2-shRNA 1#	F: 5'-CCGGGTCATCCTCATATTATCAAACCTCGAGGTTTGATAATATGAGGATGACTTTTTG-3' R: 5'-AATTCAAAAAGTCATCCTCATATTATCAAACCTCGAGGTTTGATAATATGAGGATGAC-3'
PRKAA2-shRNA2#	F: 5'-CCGGCAACTTTACCTGGTTGATAACCTCGAGGTTATCAACCAGGTAAAGTTGTTTTTG-3' R:5'-AATTCAAAAACAACTTTACCTGGTTGATAACCTCGAGGTTATCAACCAGGTAAAGTTG-3'

CRISPR/Cas9, clustered regularly interspaced short palindromic repeats/CRISPR-associated protein 9; sgRNA, single guide RNA.

Hoechst. At last, cells on slides were photographed with a confocal microscope (LSM 510 NLO; Zeiss, Oberkochen, Germany). The antibody used against ARID1A was from Sigma-Aldrich (HPA005456), the antibody used against cleaved caspase-3 was from Cell Signaling Technology (9664), and the antibodies against PRKAA2, USP9X, HDAC1, and Flag were the same as for Western blot.

Luciferase Reporter Assay

HEK293T or HCC cells were placed in a 24-well plate, 500 ng HDAC1, ARID1A-WT, ARID1A-1989* plasmid or empty vector, 200 ng *USP9X* reporter plasmid, and 20 ng renilla luciferase were co-transfected into cells for 48 hours.

Table 5. Primers for Real-Time Quantitative PCR

Primer	Sequence
Human-ARID1A	F: 5'-CCTGAAGAACTCGAACGGGAA-3' R: 5'-TCCGCCATGTTGTTGGTGG-3'
Human-USP9X	F: 5'-TCGGAGGGAATGACAACCAG-3' R: 5'-GGAGTTGCCGGGGAATTTTCA-3'
Human-PRKAA1	F: 5'-TTGAAACCTGAAAATGTCCTGCT-3' R: 5'-GGTGAGCCACAACTTGTTCTT-3'
Human-PRKAA2	F: 5'-GTGAAGATCGGACACTACGTG-3' R: 5'-CTGCCACTTTATGGCCTGTTA-3'
Human-GAPDH	F: 5'-ATGACCCCTTCATTGACCTCA-3' R: 5'-GAGATGATGACCCTTTTGGCT-3'
Mouse-Arid1a	F: 5'-TGGGACTAACCCATACTCGCA-3' R: 5'-GAATCTGCTGTGCATAAGAGAGG-3'
Mouse-Usp9x	F: 5'-GAAGCATGTCAGCGATTTTTCC-3' R: 5'-CTTAGCCACACATAGCTCCAC-3'
Mouse-Prkaa1	F: 5'-GTCAAAGCCGACCCAATGATA-3' R: 5'-CGTACACGCAAATAATAGGGGTT-3'
Mouse-Prkaa2	F: 5'-ACAGGCCATAAAGTGGCAGTT-3' R: 5'-AAAAGTCTGTCGGAGTGCTGA-3'
Mouse-Gapdh	F: 5'-AGGTCGGTGTGAACGGATTTG-3' R: 5'-GGGGTCGTTGATGGCAACA-3'

GAPDH, glyceraldehyde-3-phosphate dehydrogenase.

Then, cells were lysed by passive lysis buffer (Promega), and reporter activities were investigated by the Dual-Luciferase Reporter Assay System (Promega). The experiments were performed in triplicate.

Crystal Violet Assay and Cell Viability Assay

The crystal violet assay was performed to examine cell growth. A total of 10^4 of control cells and experimental cells were seeded in 6-well plates and cultured in medium supplemented with 10% fetal bovine serum (FBS) and 25 mmol/L glucose. The medium was changed every other day. After 10 days of culture under standard conditions, the medium was removed, and the cells were stained with a 0.5% crystal violet solution in 20% methanol and photographed. Cell viability was examined by the cell counting kit-8 or MTT assay. In short, 5×10^3 of control cells and experimental cells were seeded in 96-well plates and cultured in medium supplemented with 10% FBS and 25 mmol/L glucose. After 48 or 72 hours, the cell counting kit-8 was added for 2 hours and measured at OD 450 nm. For the MTT assay, 20 μL of 5 mg/mL MTT was added to 96-well plates for 4 hours according to the experimental design daily. At last, 200 μL dimethyl sulfoxide was added to dissolve the cell debris and detected at OD 490 nm. For the nutritional deprivation test, medium containing different doses of glucose or different content FBS were used. For the drug-response assays, different doses of Compound C (T6146) or WP1130 (T6300), both of which were purchased from Topscience (Shanghai, China), were used in complete medium.

Apoptosis Assay

Cells (5×10^5) were seeded in 6-well plates and cultured in medium with or without glucose treated with Compound C or WP1130 for 24 hours, collected, and stained using fluorescein isothiocyanate–Annexin V/Propidium iodide (PI) reagent (BD Pharmingen, San Jose, CA), followed by fluorescence-activated cell sorter analysis for the apoptotic cell population.

Table 6. ChIP Primers of the *USP9X* Promotor

Primer	Sequence
ChIP primer 1 (-1480 ~ -1377 bp)	F: 5'-GCATGCCATTTGATGTCCACAG-3' R: 5'-GTACAGTCTACCTAGGATGCCC-3'
ChIP primer 2 (-1285 ~ -1179 bp)	F: 5'-GACACAGCGGATGGGTTCATA-3' R: 5'-AGCGAATAGGCCGTACTTGA-3'
ChIP primer 3 (-986 ~ -903 bp)	F: 5'-TGGGGAAAAGGACCTCACT-3' R: 5'-ACCTGCTTGGCGCCGATAG-3'
ChIP primer 4 (-463 ~ -376 bp)	F: 5'-AGGATTTCTGGCCGTAGCAC-3' R: 5'-GAGGGGAAGACAATGCGGTA-3'
ChIP primer-ad1 (-921 ~ -841 bp)	F: 5'-CTATCGGCGCCAAGCAGG-3' R: 5'-ACGTGACGCACGAGCTG-3'

GST Pull-Down Assay

GST–HDAC1 protein were purified. Then, 5 μg GST or GST–HDAC1 proteins were added into cell lysis, which had transfected with 10 μg Flag–ARID1A before, overnight at 4°C, followed by the addition of glutathione–Sepharose 4B beads for 3 hours. After removal of nonspecific binding proteins, beads were eluted with 2 × SDS loading buffer. Proteins were examined by SDS–polyacrylamide gel electrophoresis and Western blot.

Table 7. Primers for the Nucleosome Scanning Assay

Primer	Sequence
Primer 1	F: 5'-ACAGAATTGGTGAGAGGGGACATC-3' R: 5'-ATGATTTGCCCGAAGTCAGGATT-3'
Primer 2	F: 5'-CCAATCCTGACTTCGGGCAA-3' R: 5'-AAAAAGCAGACACGACCACC-3'
Primer 3	F: 5'-GGGTGGTCGTGTCTGCTTTT-3' R: 5'-ATCCAAGATGTATCATTCATAGCCC-3'
Primer 4	F: 5'- AGGGCTATGAATGATACATCTTGGA-3' R: 5'-AGGTGACAGTGAAAGCAAGT-3'
Primer 5	F: 5'-GTCACCTACATTAGTTTGGTTCC-3' R: 5'-GGACATCAAATGGCATGCAAAATC-3'
Primer 6	F: 5'-GATTTTGCATGCCATTTGATGTC-3' R: 5'-ATTAATGGGGTGCTTGGAACA-3'
Primer 7	F: 5'-CATTTGGGCATCCTAGGTAGACT-3' R: 5'-CCAAAGTGCGGGCATAGGAAA-3'
Primer 8	F: 5'-CTATGCCCGCACTTTGGAAT-3' F: 5'-TAGGCCGTACTTGATGTGGC-3'
Primer 9	F: 5'-TATTCGCTAAGCCGTCTGGG-3' R: 5'-AGGCGTCCTCAAAGCGTTTA-3'
Primer 10	F: 5'-AAACGCTTTGAGGACGCCTA-3' R: 5'-GAAGGTGTGGCTATCTCCCG-3'
Primer 11	F: 5'-CGCTGCGGGAGATAGCCACA-3' R: 5'-CCACACCTTCCCCCTATCGGC-3'
Primer 12	F: 5'-GATCTCATCTTTCCGCGCCC-3' R: 5'-CCGACAAGAACCCGGATGAT-3'
Prime 13	F: 5'-ATCATCCGGGTTCTTGTCGG-3' R: 5'-ACGACAGGGTTAATCGCGTG-3'
Primer 14	F: 5'-TCACGCGATTAACCCTGTCG-3' R: 5'-GGCTCTAGGACCGAAGTTGG-3'
Primer 15	F: 5'-TTCGGTCCTAGAGCCACCTC-3' R: 5'-CGCGCAGTACTGTTTCTTCC-3'
Primer 16	F: 5'-AGGATTTCTGGCCGTAGCAC-3' R: 5'-GAGGGGAAGACAATGCGGTA-3'
Primer 17	F: 5'-CGCGAACAATCTTTACCGCA-3' R: 5'-CGTCAAGGCTGGGAGAGC-3'
Primer 18	F: 5'-CTGCTCTCCCAGCCTTGAC-3' R: 5'-CCCAAGACCCGAAGTTCTCC-3'
Primer 19	F: 5'-CTCTGGGGCTAGTGGGAGTC-3' R: 5'-CGTCCTCGTCAATATGGCGG-3'

ChIP

Cells were fixed and cross-linked with formaldehyde at 37°C for 10 minutes and neutralized with 125 mmol/L glycine for 5 minutes, resuspended with 500 μL lysis buffer (50 mmol/L Tris [pH = 8.1], 10 mmol/L EDTA, 1 mmol/L phenylmethylsulfonyl fluoride, and 1% SDS). The genome was fragmented by sonication under the following conditions: sonicated for 5 seconds under 300 W power at 4°C and suspended for 10 seconds, repeating these steps 6 times. After centrifugation, 5 μL supernatants were used as inputs, and the remainder was diluted 4-fold in IP buffer (20 mmol/L Tris-HCl [pH = 8.1], 2 mmol/L EDTA, 100 mmol/L NaCl, and 0.5% Triton X-100). This diluted suspension was precleared by the herring sperm DNA/Protein G–Sepharose slurry. After centrifugation, the supernatant was mixed with herring sperm DNA and Protein G–Sepharose beads and incubated with ChIP grade antibody or control IgG for 4 hours. Precipitates were washed with Buffer I (2 mmol/L EDTA, 150 mmol/L NaCl, 0.1% SDS, 1% Triton X-100, 20 mmol/L Tris-HCl [pH = 8.0]) 3 times, and Buffer II (10 mmol/L Tris-HCl [pH = 8.0], 1 mmol/L EDTA, 1% deoxycholate, 1% NP-40, 0.25 mol/L LiCl) once. Precipitated chromatin complexes were removed from beads by incubating with 150 μL dilution buffer (1.1 mol/L $NaHCO_3$ and 1% SDS). Cross-linking was reversed by incubation at 65°C for 4 hours and DNA was purified with quick columns (Qiagen, Germantown, MD). ChIP products were tested by quantitative PCR using the Thermo Scientific detection system (PIKOREAL96) with 2 × SYBR Green kit (Yeasen Biotech). The primers used are listed in Table 6. Antibodies in the ChIP experiment against ARID1A (123549), acetyl–histone H3 (Lys9) (9649), acetyl–histone H3 (Lys9) (8173), and HDAC1 (34589) were purchased from Cell Signaling Technology; antibody against Flag was purchased from Sigma-Aldrich.

Nucleosome Scanning Assay

This assay was performed as previously described.[47,48] Nucleosomal DNA was prepared by the Nucleosome Preparation Kit (Active Motif, Carlsbad, CA). Nineteen pairs of overlapping primers were used in this assay (Table 7).

Statistical Analysis

The correlations between the clinicopathologic features and ARID1A staining scores were analyzed using the chi-squared test. Survival curves were plotted by the Kaplan–Meier method and analyzed by the log-rank test. Statistical analyses were performed by GraphPad (La Jolla, CA) Prism 8 and SPSS22 software (IBM, Armonk, NY). The results are representative of at least 3 independent experiments performed in triplicate and are expressed as

the means ± SD. The data were analyzed using the Student *t* test.

References

1. Siegel RL, Miller KD, Jemal A. Cancer statistics, 2020. CA Cancer J Clin 2020;70:7–30.
2. Marquardt JU, Andersen JB, Thorgeirsson SS. Functional and genetic deconstruction of the cellular origin in liver cancer. Nat Rev Cancer 2015;15:653–667.
3. Ringelhan M, Pfister D, O'Connor T, Pikarsky E, Heikenwalder M. The immunology of hepatocellular carcinoma. Nat Immunol 2018;19:222–232.
4. Arzumanyan A, Reis HM, Feitelson MA. Pathogenic mechanisms in HBV- and HCV-associated hepatocellular carcinoma. Nat Rev Cancer 2013;13:123–135.
5. Gordan JD, Kennedy EB, Abou-Alfa GK, Beg MS, Brower ST, Gade TP, Goff L, Gupta S, Guy J, Harris WP, Iyer R, Jaiyesimi I, Jhawer M, Karippot A, Kaseb AO, Kelley RK, Knox JJ, Kortmansky J, Leaf A, Remak WM, Shroff RT, Sohal DPS, Taddei TH, Venepalli NK, Wilson A, Zhu AX, Rose MG. Systemic therapy for advanced hepatocellular carcinoma: ASCO guideline. J Clin Oncol 2020;38:4317–4345.
6. Nagarajan S, Rao SV, Sutton J, Cheeseman D, Dunn S, Papachristou EK, Prada JG, Couturier DL, Kumar S, Kishore K, Chilamakuri CSR, Glont SE, Archer Goode E, Brodie C, Guppy N, Natrajan R, Bruna A, Caldas C, Russell A, Siersbaek R, Yusa K, Chernukhin I, Carroll JS. ARID1A influences HDAC1/BRD4 activity, intrinsic proliferative capacity and breast cancer treatment response. Nat Genet 2020;52:187–197.
7. Shen J, Ju Z, Zhao W, Wang L, Peng Y, Ge Z, Nagel ZD, Zou J, Wang C, Kapoor P, Ma X, Ma D, Liang J, Song S, Liu J, Samson LD, Ajani JA, Li GM, Liang H, Shen X, Mills GB, Peng G. ARID1A deficiency promotes mutability and potentiates therapeutic antitumor immunity unleashed by immune checkpoint blockade. Nat Med 2018;24:556–562.
8. Xu G, Chhangawala S, Cocco E, Razavi P, Cai Y, Otto JE, Ferrando L, Selenica P, Ladewig E, Chan C, Da Cruz Paula A, Witkin M, Cheng Y, Park J, Serna-Tamayo C, Zhao H, Wu F, Sallaku M, Qu X, Zhao A, Collings CK, D'Avino AR, Jhaveri K, Koche R, Levine RL, Reis-Filho JS, Kadoch C, Scaltriti M, Leslie CS, Baselga J, Toska E. ARID1A determines luminal identity and therapeutic response in estrogen-receptor-positive breast cancer. Nat Genet 2020;52:198–207.
9. Shen J, Peng Y, Wei L, Zhang W, Yang L, Lan L, Kapoor P, Ju Z, Mo Q, Shih Ie M, Uray IP, Wu X, Brown PH, Shen X, Mills GB, Peng G. ARID1A deficiency impairs the DNA damage checkpoint and sensitizes cells to PARP inhibitors. Cancer Discov 2015;5:752–767.
10. Cancer Genome Atlas Research Network. Comprehensive molecular characterization of clear cell renal cell carcinoma. Nature 2013;499:43–49.
11. Guichard C, Amaddeo G, Imbeaud S, Ladeiro Y, Pelletier L, Maad IB, Calderaro J, Bioulac-Sage P, Letexier M, Degos F, Clement B, Balabaud C, Chevet E, Laurent A, Couchy G, Letouze E, Calvo F, Zucman-Rossi J. Integrated analysis of somatic mutations and focal copy-number changes identifies key genes and pathways in hepatocellular carcinoma. Nat Genet 2012;44:694–698.
12. Bitler BG, Aird KM, Garipov A, Li H, Amatangelo M, Kossenkov AV, Schultz DC, Liu Q, Shih Ie M, Conejo-Garcia JR, Speicher DW, Zhang R. Synthetic lethality by targeting EZH2 methyltransferase activity in ARID1A-mutated cancers. Nat Med 2015;21:231–238.
13. Hu C, Li W, Tian F, Jiang K, Liu X, Cen J, He Q, Qiu Z, Kienast Y, Wang Z, Zhang H, Ji Y, Hu J, Hui L. Arid1a regulates response to anti-angiogenic therapy in advanced hepatocellular carcinoma. J Hepatol 2018;68:465–475.
14. Kimura Y, Fukuda A, Ogawa S, Maruno T, Takada Y, Tsuda M, Hiramatsu Y, Araki O, Nagao M, Yoshikawa T, Ikuta K, Yoshioka T, Wang Z, Akiyama H, Wright CV, Takaori K, Uemoto S, Chiba T, Seno H. ARID1A maintains differentiation of pancreatic ductal cells and inhibits development of pancreatic ductal adenocarcinoma in mice. Gastroenterology 2018;155:194–209 e2.
15. Sun X, Wang SC, Wei Y, Luo X, Jia Y, Li L, Gopal P, Zhu M, Nassour I, Chuang JC, Maples T, Celen C, Nguyen LH, Wu L, Fu S, Li W, Hui L, Tian F, Ji Y, Zhang S, Sorouri M, Hwang TH, Letzig L, James L, Wang Z, Yopp AC, Singal AG, Zhu H. Arid1a has context-dependent oncogenic and tumor suppressor functions in liver cancer. Cancer Cell 2017;32:574–589 e6.
16. Wu C, Lyu J, Yang EJ, Liu Y, Zhang B, Shim JS. Targeting AURKA-CDC25C axis to induce synthetic lethality in ARID1A-deficient colorectal cancer cells. Nat Commun 2018;9:3212.
17. Shackelford DB, Shaw RJ. The LKB1-AMPK pathway: metabolism and growth control in tumour suppression. Nat Rev Cancer 2009;9:563–575.
18. Steinberg GR, Carling D. AMP-activated protein kinase: the current landscape for drug development. Nat Rev Drug Discov 2019;18:527–551.
19. Eichner LJ, Brun SN, Herzig S, Young NP, Curtis SD, Shackelford DB, Shokhirev MN, Leblanc M, Vera LI, Hutchins A, Ross DS, Shaw RJ, Svensson RU. Genetic analysis reveals AMPK is required to support tumor growth in murine Kras-dependent lung cancer models. Cell Metab 2019;29:285–302 e7.
20. Jeon SM, Chandel NS, Hay N. AMPK regulates NADPH homeostasis to promote tumour cell survival during energy stress. Nature 2012;485:661–665.
21. Lee H, Zandkarimi F, Zhang Y, Meena JK, Kim J, Zhuang L, Tyagi S, Ma L, Westbrook TF, Steinberg GR, Nakada D, Stockwell BR, Gan B. Energy-stress-mediated AMPK activation inhibits ferroptosis. Nat Cell Biol 2020;22:225–234.
22. Zhang D, Wang W, Sun X, Xu D, Wang C, Zhang Q, Wang H, Luo W, Chen Y, Chen H, Liu Z. AMPK regulates autophagy by phosphorylating BECN1 at threonine 388. Autophagy 2016;12:1447–1459.
23. Ogiwara H, Takahashi K, Sasaki M, Kuroda T, Yoshida H, Watanabe R, Maruyama A, Makinoshima H, Chiwaki F, Sasaki H, Kato T, Okamoto A, Kohno T. Targeting the

vulnerability of glutathione metabolism in ARID1A-deficient cancers. Cancer Cell 2019;35:177–190 e8.
24. Finicle BT, Jayashankar V, Edinger AL. Nutrient scavenging in cancer. Nat Rev Cancer 2018;18:619–633.
25. Chhipa RR, Fan Q, Anderson J, Muraleedharan R, Huang Y, Ciraolo G, Chen X, Waclaw R, Chow LM, Khuchua Z, Kofron M, Weirauch MT, Kendler A, McPherson C, Ratner N, Nakano I, Dasgupta N, Komurov K, Dasgupta B. AMP kinase promotes glioblastoma bioenergetics and tumour growth. Nat Cell Biol 2018;20:823–835.
26. Mihaylova MM, Shaw RJ. The AMPK signalling pathway coordinates cell growth, autophagy and metabolism. Nat Cell Biol 2011;13:1016–1023.
27. Deng M, Yang X, Qin B, Liu T, Zhang H, Guo W, Lee SB, Kim JJ, Yuan J, Pei H, Wang L, Lou Z. Deubiquitination and activation of AMPK by USP10. Mol Cell 2016;61:614–624.
28. Lee MS, Han HJ, Han SY, Kim IY, Chae S, Lee CS, Kim SE, Yoon SG, Park JW, Kim JH, Shin S, Jeong M, Ko A, Lee HY, Oh KJ, Lee YH, Bae KH, Koo SH, Kim JW, Seong JK, Hwang D, Song J. Loss of the E3 ubiquitin ligase MKRN1 represses diet-induced metabolic syndrome through AMPK activation. Nat Commun 2018;9:3404.
29. Vila IK, Yao Y, Kim G, Xia W, Kim H, Kim SJ, Park MK, Hwang JP, Gonzalez-Billalabeitia E, Hung MC, Song SJ, Song MS. A UBE2O-AMPKalpha2 axis that promotes tumor initiation and progression offers opportunities for therapy. Cancer Cell 2017;31:208–224.
30. Yonezawa T, Kurata R, Kimura M, Inoko H. Which CIDE are you on? Apoptosis and energy metabolism. Mol Biosyst 2011;7:91–100.
31. Driessen S, Berleth N, Friesen O, Loffler AS, Bohler P, Hieke N, Stuhldreier F, Peter C, Schink KO, Schultz SW, Stenmark H, Holland P, Simonsen A, Wesselborg S, Stork B. Deubiquitinase inhibition by WP1130 leads to ULK1 aggregation and blockade of autophagy. Autophagy 2015;11:1458–1470.
32. Schick S, Rendeiro AF, Runggatscher K, Ringler A, Boidol B, Hinkel M, Majek P, Vulliard L, Penz T, Parapatics K, Schmidl C, Menche J, Boehmelt G, Petronczki M, Muller AC, Bock C, Kubicek S. Systematic characterization of BAF mutations provides insights into intracomplex synthetic lethalities in human cancers. Nat Genet 2019;51:1399–1410.
33. Schwickart M, Huang X, Lill JR, Liu J, Ferrando R, French DM, Maecker H, O'Rourke K, Bazan F, Eastham-Anderson J, Yue P, Dornan D, Huang DC, Dixit VM. Deubiquitinase USP9X stabilizes MCL1 and promotes tumour cell survival. Nature 2010;463:103–107.
34. Perez-Mancera PA, Rust AG, van der Weyden L, Kristiansen G, Li A, Sarver AL, Silverstein KA, Grutzmann R, Aust D, Rummele P, Knosel T, Herd C, Stemple DL, Kettleborough R, Brosnan JA, Li A, Morgan R, Knight S, Yu J, Stegeman S, Collier LS, ten Hoeve JJ, de Ridder J, Klein AP, Goggins M, Hruban RH, Chang DK, Biankin AV, Grimmond SM, Australian Pancreatic Cancer Genome I, Wessels LF, Wood SA, Iacobuzio-Donahue CA, Pilarsky C, Largaespada DA, Adams DJ, Tuveson DA. The deubiquitinase USP9X suppresses pancreatic ductal adenocarcinoma. Nature 2012;486:266–270.
35. Dreval K, Lake RJ, Fan HY. HDAC1 negatively regulates selective mitotic chromatin binding of the Notch effector RBPJ in a KDM5A-dependent manner. Nucleic Acids Res 2019;47:4521–4538.
36. Huang, Li T, Wang L, Zhang L, Yan R, Li K, Xing S, Wu G, Hu L, Jia W, Lin SC, Dang CV, Song L, Gao P, Zhang H. Hepatocellular carcinoma redirects to ketolysis for progression under nutrition deprivation stress. Cell Res 2016;26:1112–1130.
37. Hwang SH, Kim MC, Ji S, Yang Y, Jeong Y, Kim Y. Glucose starvation induces resistance to metformin through the elevation of mitochondrial multidrug resistance protein 1. Cancer Sci 2019;110:1256–1267.
38. Zong Y, Zhang CS, Li M, Wang W, Wang Z, Hawley SA, Ma T, Feng JW, Tian X, Qi Q, Wu YQ, Zhang C, Ye Z, Lin SY, Piao HL, Hardie DG, Lin SC. Hierarchical activation of compartmentalized pools of AMPK depends on severity of nutrient or energy stress. Cell Res 2019;29:460–473.
39. Pineda CT, Ramanathan S, Fon Tacer K, Weon JL, Potts MB, Ou YH, White MA, Potts PR. Degradation of AMPK by a cancer-specific ubiquitin ligase. Cell 2015;160:715–728.
40. Liu H, Ding J, Kohnlein K, Urban N, Ori A, Villavicencio-Lorini P, Walentek P, Klotz LO, Hollemann T, Pfirrmann T. The GID ubiquitin ligase complex is a regulator of AMPK activity and organismal lifespan. Autophagy 2020;16:1618–1634.
41. Jia J, Bissa B, Brecht L, Allers L, Choi SW, Gu Y, Zbinden M, Burge MR, Timmins G, Hallows K, Behrends C, Deretic V. AMPK, a regulator of metabolism and autophagy, is activated by lysosomal damage via a novel galectin-directed ubiquitin signal transduction system. Mol Cell 2020;77:951–969 e9.
42. Jia J, Bissa B, Brecht L, Allers L, Choi SW, Gu Y, Zbinden M, Burge MR, Timmins G, Hallows K, Behrends C, Deretic V. AMPK is activated during lysosomal damage via a galectin-ubiquitin signal transduction system. Autophagy 2020;16:1550–1552.
43. Williamson CT, Miller R, Pemberton HN, Jones SE, Campbell J, Konde A, Badham N, Rafiq R, Brough R, Gulati A, Ryan CJ, Francis J, Vermulen PB, Reynolds AR, Reaper PM, Pollard JR, Ashworth A, Lord CJ. ATR inhibitors as a synthetic lethal therapy for tumours deficient in ARID1A. Nat Commun 2016;7:13837.
44. Liu Z, Zhang G, Huang S, Cheng J, Deng T, Lu X, Adeshakin FO, Chen Q, Wan X. Induction of apoptosis in hematological cancer cells by dorsomorphin correlates with BAD upregulation. Biochem Biophys Res Commun 2020;522:704–708.
45. Ali JL, Lagasse BJ, Minuk AJ, Love AJ, Moraya AI, Lam L, Arthur G, Gibson SB, Morrison LC, Werbowetski-Ogilvie TE, Fu Y, Nachtigal MW. Differential cellular responses induced by dorsomorphin and LDN-193189 in chemotherapy-sensitive and chemotherapy-resistant

human epithelial ovarian cancer cells. Int J Cancer 2015; 136:E455–E469.
46. Liu X, Chhipa RR, Nakano I, Dasgupta B. The AMPK inhibitor compound C is a potent AMPK-independent antiglioma agent. Mol Cancer Ther 2014;13: 596–605.
47. Gupta Piyushi, Singh Ankita, Gowda Pruthvi, Ghosh Sadashib, Chatterjee Arpita, Sen Ellora, et al. Lactate induced HIF-1α-PRMT1 cross talk affects MHC I expression in monocytes. Exp Cell Res 2016; 347(2):293–300.
48. Sheikh Touseef, Sen Ellora. p53 affects epigenetic signature on SOCS1 promoter in response to TLR4 inhibition. Cytokine 2021;140:155418, 155418.

Received September 27, 2021. Accepted March 28, 2022.

Correspondence
Address correspondence to: Jing-Jing Li, PhD, or Dong Xie, PhD, Shanghai Institute of Nutrition and Health, Chinese Academy of Sciences, 320 YueYang Road, Shanhgai 200031, China. e-mail: tide7@163.com; fax: (86) 21-54920078.

Acknowledgments
The authors thank the New World Group for their Charitable Foundation to establish the Institute for Nutritional Sciences, Shanghai Institutes for Biological Sciences (SIBS), Chinese Academy of Sciences (CAS)–New World Joint Laboratory, which have given full support to this study.

The authors greatly appreciate the kind gift of *USP9X* plasmid from Professor Yong-Jun Dang (School of Basic Medical Sciences, Fudan University).

CRediT Authorship Contributions
Feng-Kun Zhang (Data curation: Lead; Methodology: Lead; Software: Lead; Visualization: Lead; Writing – original draft: Lead)
Qian-Zhi Ni (Investigation: Equal)
Kang Wang (Methodology: Supporting)
Hui-Jun Cao (Investigation: Supporting)
Dongxian Guan (Methodology: Equal)
Er-Bin Zhang (Data curation: Supporting)
Ning Ma (Formal analysis: Supporting)
Yi-Kang Wang (Methodology: Supporting)
Qian-Wen Zheng (Resources: Supporting)
Sheng Xu (Software: Supporting)
Bing Zhu (Validation: Supporting)
Tian-Wei Chen (Software: Supporting)
Ji Xia (Resources: Supporting)
Xiao-Song Qiu (Software: Supporting)
Xu-Fen Ding (Validation: Supporting)
Hao Jiang (Investigation: Supporting)
Lin Qiu (Software: Supporting)
Xiang Wang (Visualization: Supporting)
Wei Chen (Resources: Supporting)
Shu-Qun Cheng (Supervision: Supporting)
Dong Xie (Conceptualization: Lead; Funding acquisition: Lead)
Jingjing Li, PhD (Conceptualization: Lead; Funding acquisition: Lead; Supervision: Lead)

Conflicts of interest
The authors disclose no conflicts.

Funding
This work was supported by National Natural Science Foundation of China grants 31771538, 81972757, and 82172950; Youth Innovation Promotion Association of Chinese Academy of Sciences grant 2017324; Sanofi-SIBS 2018 Young Faculty Award (J.-J.L.); National Natural Science Foundation of China grants 81730083 and 82030084; and the National Key R&D Program of China grants 2018YFC1604404 and 2018YFC1603002 (D.X.).